

A Novel Precast Concrete Beam–Column Connection With Replaceable Energy-Dissipation Connector: Experimental Investigation and Theoretical Analysis

Chao Tong

Southeast University

Jing Wu (✉ seuwj@seu.edu.cn)

Southeast University

Chunyu Li

Shijiazhuang Tiedao University

Research Article

Keywords: precast concrete beam–column connection, additional bending moment, replaceable energy-dissipation connector, energy-dissipation capacity, load capacity

Posted Date: February 23rd, 2021

DOI: <https://doi.org/10.21203/rs.3.rs-219155/v1>

License: © ⓘ This work is licensed under a Creative Commons Attribution 4.0 International License.

[Read Full License](#)

1 **A novel precast concrete beam–column connection with replaceable**
2 **energy-dissipation connector: Experimental investigation and**
3 **theoretical analysis**

4 Chao Tong¹, Jing Wu¹, Chunyu Li^{1,2}

5 ¹ The Key Laboratory on Concrete and Prestressed Concrete Structures of Ministry of Education of China,
6 Southeast University, Nanjing, China

7 ² School of Civil Engineering, Shijiazhuang Tiedao University, Shijiazhuang 050043, China

8
9 **Abstract:** In order to avoid the damage of the connection due to the overstrength of beam
10 strength, and the alternation of the strength hierarchy in the structural system. The additional
11 bending moment produced by the combined action of the pressure generated by the concrete
12 compression zone and the tension generated by the reinforcements needs to be reduced. A novel
13 precast concrete beam–column connection is proposed herein. In the proposed connection, the
14 precast beam is laid on a steel corbel embedded in the precast column. A novel replaceable energy-
15 dissipation connector (REDC) is placed at the bottom of the steel corbel, which ensures that it is
16 in the same horizontal position aligned with the longitudinal reinforcement at the bottom of the
17 connection. In addition, there is a narrow vertical slot adjacent to the column face. The total yield
18 capacity of the top reinforcement is larger than that of the bottom REDC energy-dissipation
19 connector. Theory study focused on the structural features and mechanical mechanism of this novel
20 precast connection. Three low-cycle quasi-static loading tests were carried out on a single full-

1 scaled specimen by replacing three REDCs with different sizes. The cracking pattern of this novel
2 precast connection, and the effects of different parameters of the REDCs on the energy-dissipation
3 capacity and load capacity of the connections were discussed. By performing a finite-element
4 simulation, a method for reducing the additional bending moment and keeping the top
5 reinforcements always in elastic was developed. In addition, the relevant design suggestions were
6 provided. The conclusion shows that the seismic performance of this novel precast concrete beam–
7 column connection is excellent. The positive and negative bending moments of novel precast
8 concrete beam–column connection both reduce the additional bending moment. In view of this,
9 the bending moment of the novel connection is a controllable variable.

10 **Keywords:** precast concrete beam–column connection; additional bending moment; replaceable
11 energy-dissipation connector; energy-dissipation capacity; load capacity.

13 **1. Introduction**

14 In recent years, the precast concrete structure has been developed comprehensively and has
15 gradually replaced the traditional cast-in-place structure. It promotes the process of construction
16 industrialization and satisfies the needs of the future development of the construction industry
17 (Hassoun, M. N, and Al-Manaseer, A. 2020). Although the “wet” fabricated structures can be
18 equivalent to or close to the cast-in-place structures, it inherits the characteristics of damage
19 dispersion of the cast-in-place structures under strong earthquakes (Liu H, Yan Q, Du X. 2017).
20 Under seismic action, the ductility of the plastic hinge at the beam end of the structures mainly
21 depends on the yield of the longitudinal reinforcements at the beam end. Because of the crushing

1 of concrete in the compression zone and the buckling of the longitudinal reinforcements caused by
2 the rotation of the plastic hinge, the moment capacity decreases rapidly. This type of failure occurs
3 particularly easily under the negative moment, because the height of the compression zone in the
4 bottom of the beam is relatively high. After the earthquake, although the cracked or slightly
5 crushed concrete can be repaired, the buckled or yielded longitudinal reinforcement is difficult to
6 repair or replace. Therefore, it is difficult to repair the cast-in-place structures and most of the “wet”
7 precast structures after the earthquake. Numerous seismic damage investigations revealed a
8 phenomenon of “strong beam and weak column” in structures under earthquake excitation,
9 although the seismic principle of “strong column weak beam” is universally emphasized in the
10 design philosophy. The significantly increase of the beam overstrength moments and hence column
11 moment demands, altering the hierarchy of strength such that undesirable column hinging may
12 occur, in the worst case, can result in undesirable soft-story failure (Huang et al. 2020). This is
13 mainly due to the large area of the slab reinforcement in the flange of the frame beam, which
14 contributes to the bending moment resistance together with the longitudinal reinforcement in the
15 beam when they bear the negative bending moment, resulting in an overstrength bending moment
16 of the beam. Thus, the ideal hinge mechanism cannot be realized. These are important problems
17 that must be solved for prefabricated concrete structures, particularly for “wet” prefabricated
18 concrete structures, which are equivalent to cast-in-place structures. The main reason for this
19 phenomenon is that the floor slab (similar to the flange of the beam) has a large area of
20 reinforcement, which contributes to the moment capacity together with the longitudinal
21 reinforcements in the beam. This flange effect can significantly increase the overstrength beam

1 moments, which can result in hinging of columns and the formation of an undesirable soft-story
2 mechanism. These issues affect the structural safety (Huang et al. 2020).

3 In recent decades, the seismic performance of fabricated structures has been studied deeply
4 and comprehensively. In the 1970s, Blakeley, Park (1971), and Thompson (1975) experimentally
5 investigated the joints and structures of prefabricated frames to understand their behavior under
6 cyclic load reversals. The test results indicated that prefabricated concrete structures have
7 favorable integrity, ductility properties, and deformation recovery capabilities. The Precast
8 Seismic Structural System Research Program (PRESSSS) began in 1991 and was jointly undertaken
9 by researchers in the United States and Japan. As one of the first research projects in this field, the
10 PRESSSS involved a detailed investigation of precast concrete structures (Priestley, M J Nigel. 1991;
11 Priestley, M J Nigel.1996; Priestley, M J Nigel., and Macrae G A. 1996; Vasconez R M., Naaman
12 A E, Wight J K. 1998). In 2003, the European Union initiated a seismic research project for precast
13 concrete structures based on Eurocode 8 (Fan Li., Lv Xilin, Zhao Bin. 2007), in which the seismic
14 performance of beam–column connections and frames was investigated, and useful results were
15 obtained. Nakaki et al. (1994) proposed precast concrete beam–column connections with dywidag
16 ductile connector (DDC). Englekirk (1995) tested precast concrete beam–column connections with
17 DDC ductile connectors under quasi-static cyclic loading to evaluate their seismic performance.
18 Under 3.5% interstory drift, the connections and components exhibited no obvious damage.
19 Englekirk (1996) first used the DDC ductile connector in the Wiltern Center Parking in Los
20 Angeles. This structure has been analyzed by Englekirk (2002) and applied to famous buildings,
21 including the Highland Center in Hollywood and the Paramount apartment in San Francisco. Bara

1 Chang et al. (2012, 2014) tested full-scale and scaled specimens of frames with DDC. The results
2 confirmed that the connections with the DDC had a stable energy-dissipation capacity and that the
3 seismic performance of the DDC frames was better than that of conventional frames. Kenyon et
4 al. (2008) conducted a finite-element simulation to evaluate the seismic performance of precast
5 concrete frames with a DDC.

6 Additionally, according to the Damage Avoidance Design (DAD) approach (Bacht T et al.
7 2011; Mander J B, Cheng C-T. 1997; Mander T J et al. 2009; Linjie Huang et al. 2020), various
8 yielding steel devices have been proposed and used in structures. Damage avoidance can be
9 achieved in moment frames by using special devices that do not undergo degradation of the
10 dissipative performance with use. Compared with the conventional moment frames and “wet”
11 precast frames, precast frames designed according to the DAD approach. This principle reduces
12 the amount of frame repair needed, and the minimized disruption substantially reduces the
13 economic and business impacts. Amaris et al. (2008) and Marriott (2009) proposed a tension and
14 compression yield energy-dissipation device. However, this type of energy-dissipation device is
15 installed outside the beams; thus, the transfer force is indirect and easily causes the failure of the
16 anchoring of the conversion block. Chanchi et al. (2018, 2019) tested and simulated an asymmetric
17 friction energy-dissipation device and applied it to steel structures. Rodgers (2019) tested a series
18 of lead squeeze dampers. Oh et al. (2009) and Koken et al. (2013) have tested full-scale specimens
19 of steel beam–column connections with steel slit dampers and compared them with the
20 conventional steel connections. The test results indicated that the steel slit damper provides a
21 reliable energy-dissipation capacity. Chi et al. (2012) experimentally and analytically investigated

1 the cyclic response of a post-tensioned column base connection with a buckling-restrained steel
2 plate (BRS). The results indicated that the BRS plate had good energy-dissipation capacity when
3 yielding under tension and compression. These steel energy-dissipation devices have an excellent
4 and stable energy-dissipation capacity but have disadvantages; e.g., they have a complex structure,
5 require extra space, and are difficult to replace.

6 Another consequence of plastic hinge formation is beam elongation. Over the course of a
7 significant seismic event, a plastic hinge can lengthen by 2%–5% of the beam depth (Fenwick R
8 C et al. 1995). On one hand, the beam elongation increases the flexural capacity, leading to the
9 phenomenon of “strong beam and weak column”. On the other hand, the beam elongation can
10 increase the lateral resistance of a moment resisting frame and cause significant damage to the
11 floor diaphragm (Bull. D. K. 2003; Peng et al. 2009). To solve this problem, Ohkubo et al. (2009)
12 proposed a slotted beam–column connection and performed experiments to examine the shear
13 transfer mechanism in the beam-end region. The results indicated that the slotted beams have good
14 flexural characteristics. Ohkubo et al. (2004) tested a reinforced-concrete (RC) slotted-beam
15 structure with a floor slab to investigate the damage to the floor slab. The results indicated that the
16 cracks and damage in the floor slab for slotted-beam frames were significantly reduced compared
17 with those for the conventional frames. Au (2010), J.D.R. Byrne et al. (2012), and C. A. Muir et
18 al. (2013) tested slotted-beam connections and frames and verified that the slotted-beam structures
19 had good seismic performance. Additionally, Oudah (2013) tested numerous specimens of slotted-
20 beam connections to examine the effects of the vertical slot position on the seismic performance
21 and damage to the connection. Many studies have been performed on slotted-beam connections in

1 cast-in-place concrete structures, but there have been relatively few studies on slotted-beam
2 connections in precast concrete structures. At present, the research on slotted-beam connections
3 mainly focuses on cast-in-place concrete frame structures, and there is little research on the
4 fabricated frame structures.

5 To address the aforementioned issues, this paper proposes a novel precast beam–column
6 concrete connection with a replaceable energy-dissipating connector (REDC). At the same
7 horizontal position as the longitudinal reinforcement at the bottom of the beam, the REDC energy-
8 dissipation connector is connected to the longitudinal reinforcements in the beam and column by
9 connecting blocks. The hidden corbel is used to provide a sufficient vertical shear capacity and to
10 facilitate construction of the beam and column assembly. The vertical slot is installed in the bottom
11 of the beam, adjacent to the column face, reducing the height of the compression zone. If the yield-
12 capacity ratio of the top reinforcement to the bottom REDC energy-dissipation connector is
13 increased and the height of the concrete compression zone is reduced, the neutral axis of the
14 connection will move upward, and the additional bending moment of the beam-column connection
15 will reduce. At the same time, when the frame composed by these novel connections is subjected
16 to earthquake ground motions, the damage to the structure is mainly concentrated in the REDCs.
17 After the earthquake, the structure can be repaired quickly by replacing the REDCs. Because of
18 the reducing of the additional bending moment , the moment capacity of the connection is
19 controlled by the REDCs as much as possible, and the principle of “strong column weak beam” is
20 easily realized. Therefore, the principles of “strong shear weak moment” and “strong connection
21 weak member” can be achieved. In this study, the seismic performance of the novel precast

1 connection was investigated via a theoretical analysis and experimental research, and design values
2 were recommended for the relevant parameters.

3 2. Novel precast concrete beam–column connection with REDC

4 2.1. Connection overview

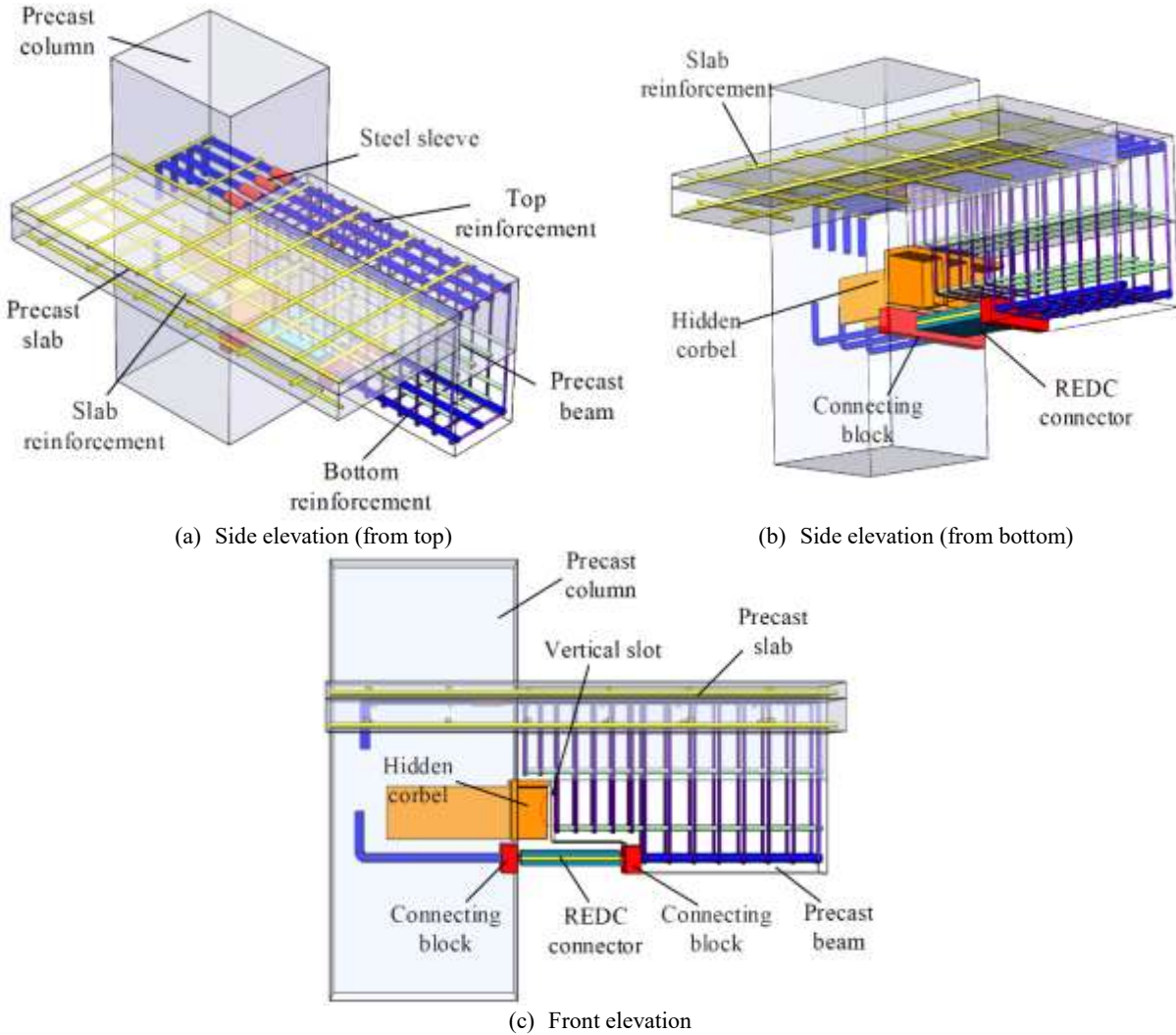


Fig 1 Description of the novel precast concrete beam–column connections with the REDC

5 A schematic configuration of the novel precast connection assembly is presented in Fig. 1.
6 The connection is composed of four main parts: the precast concrete beam, the precast concrete
7 column, the REDC, and the hidden corbel. As shown in Fig. 1(a), the top longitudinal
8 reinforcements in the connection are connected by steel sleeves. The area of the top longitudinal

1 reinforcements (containing slab reinforcements) exceeds the area of the REDC core plate. As
 2 shown in Fig. 1(b), the hidden corbel is embedded in the column and lapped with the rabbet of the
 3 precast beam. The π -shaped hidden corbel consists of two welded steel plates, which contribute to
 4 the shear and bending capacities of the corbel. At the same horizontal position as the longitudinal
 5 reinforcement at the bottom of the beam, the REDC energy-dissipation connector is connected to
 6 the longitudinal reinforcement in the beam and column by connecting blocks. As shown in Fig.
 7 1(c), the vertical slot is installed at the bottom of the beam, immediately adjacent to the column
 8 face.

9 **2.2.Details of REDC**

10

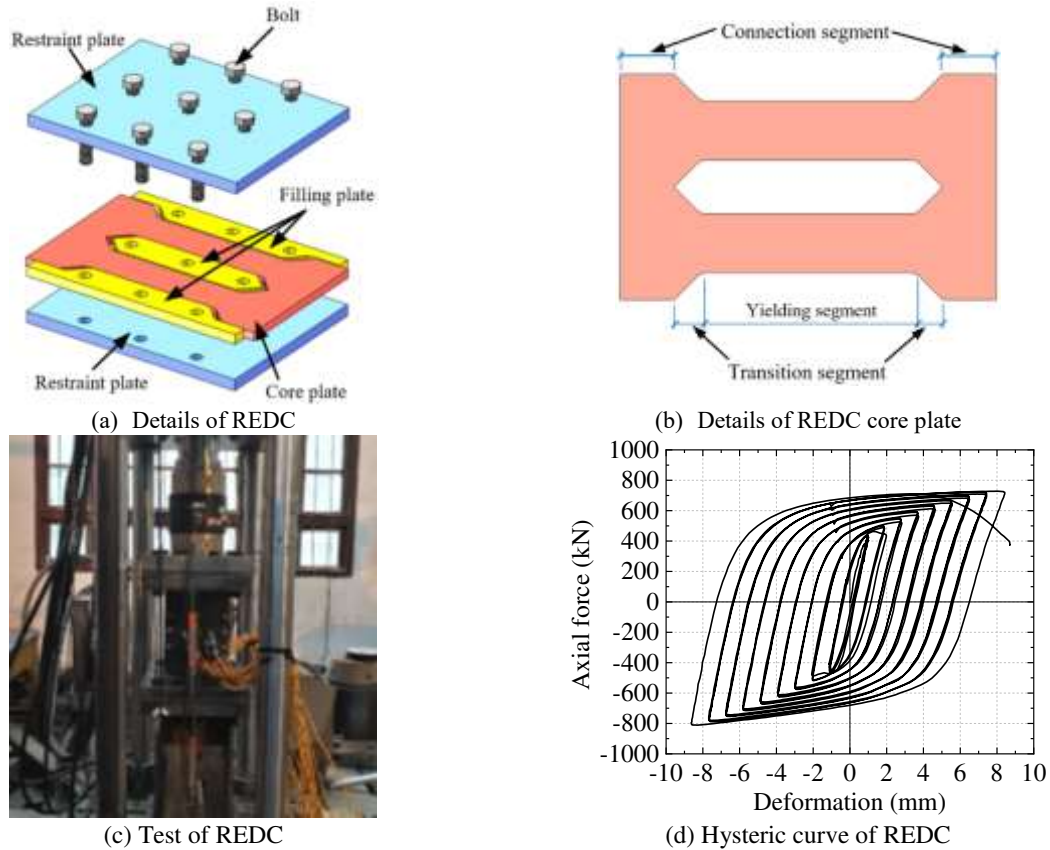


Fig 2 Details and test of REDC

11 The REDC is a buckling-restrained energy dissipater, and proposed by Xie (2020). In addition,

1 Li (2020) proposed a precast concrete frame with replaceable energy-dissipating connectors
 2 (REDC-PCF) and test it. Figs.2 (a)-(d) are details and test of REDC. The REDC is assembled by
 3 bolts and composed of a core plate, filling plate and restraint plate (Fig. 2 (a)). The core plate is
 4 welded to structural members and yields under repeated axial loads. The filling plate and restraint
 5 plate are used to avoid the compression buckling of the core plate. The section of core plate varies
 6 along the length (Fig. 2 (b)), and it is divided into yielding segment, transition segment, and
 7 connection segment. In addition, the stable hysteretic energy dissipation capability of REDC
 8 observed in an axial cyclic tension-compression test can be observed from Figs. 2 (c) and (d) (Xie.
 9 2020). The damage to the connection is mainly concentrated on the REDC. The energy-dissipation
 10 capacity of the novel precast connection is provided by the tension and compression plastic
 11 deformation of the REDC. After the earthquake, the structures can be repaired quickly by replacing
 12 the REDCs.

13 **2.3.Mechanics of the novel precast connection**

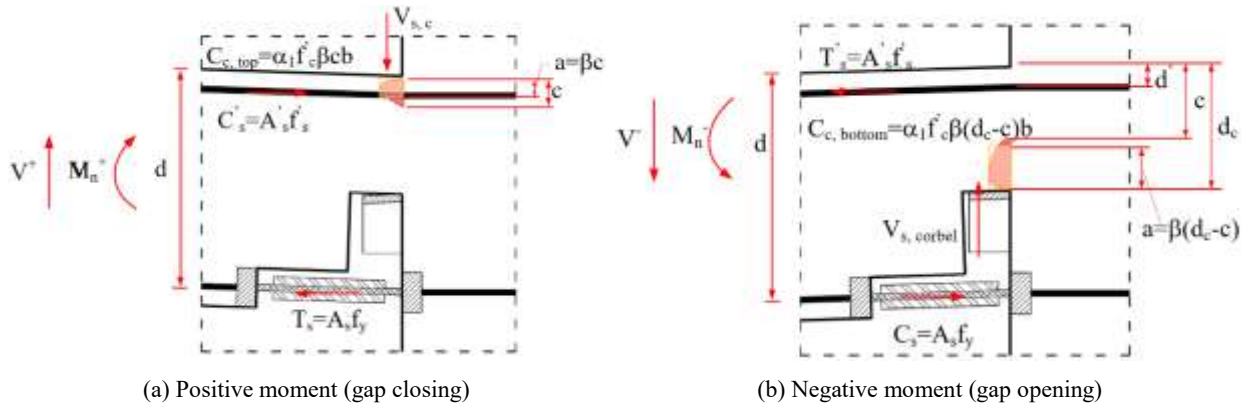


Fig. 3 Force distribution in the connection under positive and negative bending

14 Figs. 3(a) and (b) illustrate the forces in this novel precast connection at positive (gap closing)
 15 and negative (gap opening) nominal strength moments. The gap closing and opening correspond
 16 to the positive moment under the positive drift and the negative moment under the negative drift,

1 respectively.

2 The flexural response of this novel precast connection is governed by the yielding of the
3 REDC core plate and the concrete compression zone. The positive nominal flexural strength (M_n^+)
4 can be calculated similarly to that in the case of a conventional RC connection, i.e., by multiplying
5 the REDC yield force about a lever arm, as indicated by Eq. (1). This is an approximation that
6 conservatively ignores the force in the top reinforcement and any additional confinement to the
7 concrete hinge from the column face.

$$M_n^+ = A_s f_y (d - a/2) \quad (1)$$

8 where A_s represents the equivalent cross-sectional area of the REDC core plate; f_y represents the
9 yield strength of the REDC core plate; d represents the beam effective depth; a represents the
10 Whitney equivalent rectangular concrete stress block depth.

11 The flexural mechanism for negative moments in this novel precast connection differs from
12 that for conventional RC beams. There is no concrete compression at the beam soffit, owing to the
13 slot. However, there is concrete compression at the bottom of the concrete top-hinge, as shown in
14 Fig. 2(b). The negative nominal flexural strength can be accurately approximated as follows:

$$M_n^- = A_s f_y (d - d') + a_1 f'_c \beta (d_c - c) b (d_c - a/2) \quad (2)$$

15 where d' represents the depth to the top reinforcement; a_1 and β are concrete stress block factors;
16 f'_c represents the specified 28-d concrete compressive strength; d_c represents the depth of the
17 concrete top-hinge in this novel precast connection; c represents the neutral-axis depth (measured
18 from the top surface of the beam); b represents the section width of the beam.

19 For gap-opening rotations (positive moment), the shear forces transferred through the

1 compression concrete zone can be designed according to the Code for Seismic Design of Buildings
2 in China (GB50010-2010) (2010), as follows:

$$V^+ \leq V_{s,c} = 0.25\beta_c f'_c b h_0 \quad (3)$$

3 where $V_{s,c}$ is the shear forces transferred through the compression concrete zone; β_c is the
4 coefficient of concrete strength (=1.0 for C50 concrete), and h_0 represents the effective height of
5 the cross section (h_0 represents the d_c in this novel precast connection).

6 For gap-closing rotations (positive moment), the shear forces transferred via the hidden corbel
7 can be designed using Eq. (3).

$$V^- \leq V_{s, \text{corbel}} \quad (4)$$

8 where $V_{s, \text{corbel}}$ represents the shear capacity provided by the hidden corbel.

9 **3. Experimental study on the novel precast connection**

10 **3.1. Test specimen**

11 To experimentally investigate the hysteretic behavior of the novel precast connection under
12 cyclic loading, a full-scale test specimen was fabricated, as shown in Fig. 3. This specimen
13 corresponded to the exterior beam–column connection from a prototype concrete frame in China.
14 According to the Chinese Code for Seismic Design of Buildings (GB50010-2010), this frame
15 being designed is located at the area of seismic intensity 8, seismic group 1, and soil type II, with
16 a peak ground acceleration (PGA) of 0.4g for the maximum considered earthquake (MCE) (2%
17 exceedance probability in 50 years). As shown in Fig. 4(a), the column was 2800 mm tall, with a
18 cross section having dimensions of 500mm × 700 mm. The beam was 1,800 mm long, with a cross
19 section of 300 mm × 600 mm. The cross sections and reinforcement layouts of the beam and

1 column are shown in Figs. 4(b)–(e). The REDC was connected by the core plate, the restraining
2 plates, and the filler plates using bolts. The dimensions and parameters of the REDCs are shown
3 in Figs. 4(f)–(i). There were 1-mm gaps between the filler plates, restraining plates, and core plate.
4 There was a sufficient gap between the filler plates and the core plate to satisfy the compression
5 deformation of the core plate. Au (2010) proposed that when $A'_s f'_y / A_s f_y > 2.5$, the neutral axis of
6 the connection will move upward, and the top reinforcement to remain elastic. Therefore, for the
7 top longitudinal reinforcement in this novel precast connection, six 28-mm-diameter deformed
8 bars and HPB400 steel (yield stress of 400 MPa) were used to decrease the yield-capacity ratio of
9 the top reinforcement to the bottom REDC energy-dissipation connector ($A'_s f'_y / A_s f_y$). It is worth
10 noting that these six bars include the equivalent bars in the slabs. Therefore, the flange effect of
11 slabs in connection was considered by equivalent reinforcement. In addition, the thickness of the
12 REDC core plate was 14 mm. Therefore, the $A'_s f'_y / A_s f_y$ for the test specimen was 3.68 (> 2.5). To
13 simplify the construction of the specimen, the sleeve-connected top reinforcements were replaced
14 with continuous reinforcements. One π -shaped steel hidden corbel was embedded in the column,
15 at the half-height of the beam. The length of the corbel was 80 mm, and the cross section of the
16 flange plate in the π -shaped steel corbel was 300 mm \times 18 mm. The cross section of the web plates
17 in the π -shaped steel corbel was 18 mm \times 160 mm. The slot adjacent to the column face was 20
18 mm wide, which was sufficient to accommodate 4.0% drifts without contact between the beam
19 soffit and the column face. The height of the slot (the distance from the top of the corbel to the
20 bottom of the beam) was 300 mm.

21

1
2
3
4

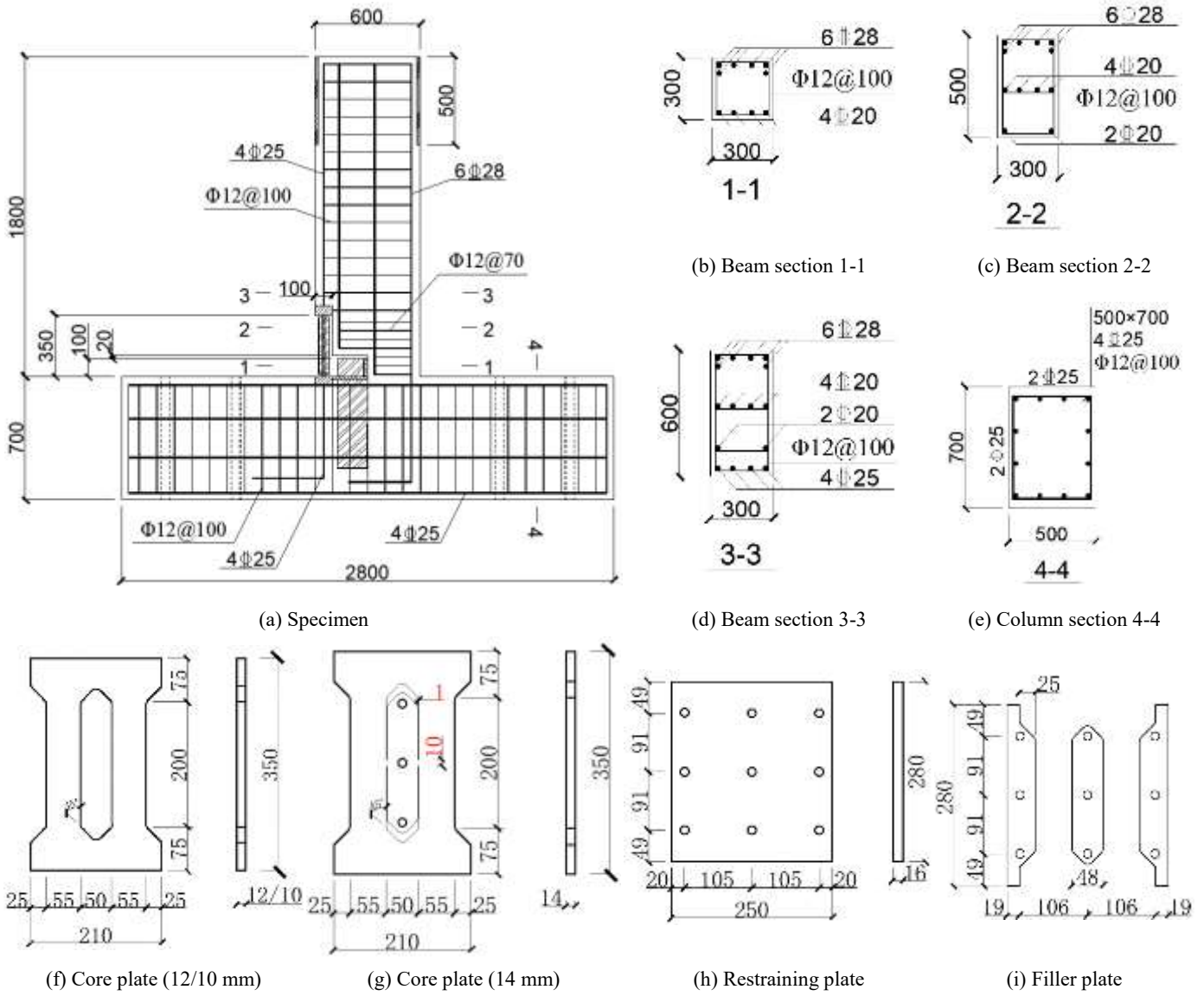


Fig. 4 Details of the tested connections (all dimensions have units of mm)

5 **3.2. Material properties**

6 For the test specimen, the material properties of the reinforcements, the π -shaped steel corbel

1 and connecting blocks are presented in Table 1.

2 **Table 1** Mechanical properties of the structural steels in the specimen

Material	Structural components	Yielding strength	Ultimate strength	Young's modulus
		f_y (MPa)	f_p (MPa)	E_s (N/mm ²)
Q345	Steel corbel and connecting blocks	443.98	586.32	211023
HRB400	Reinforcement D28	420.18	490.04	206734
HRB400	Reinforcement D25	417.21	478.92	206837
HRB400	Stirrup 14	476.12	527.33	210322

3 The grade of the concrete in the specimen was C50. Three groups of compressive-strength tests
 4 were performed, and the results are presented in Table 2. The test results all satisfied the GB50010-
 5 2010.

6 **Table 2** Cube strength of C50 concrete

Test specimen	1	2	3	Average
Strength (MPa)	60.22	51.38	53.47	55.02

7 The REDC was fabricated using the Q235 plate. Three samples of the Q235 plate were tested, and
 8 the results are presented in Table 3. In addition, the carbon dioxide gas shielded arc welding is
 9 used to weld the core plate and the connecting blocks, and the type of welding wire is ER50-6.

10 **Table 3** Material test results for Q235 steel

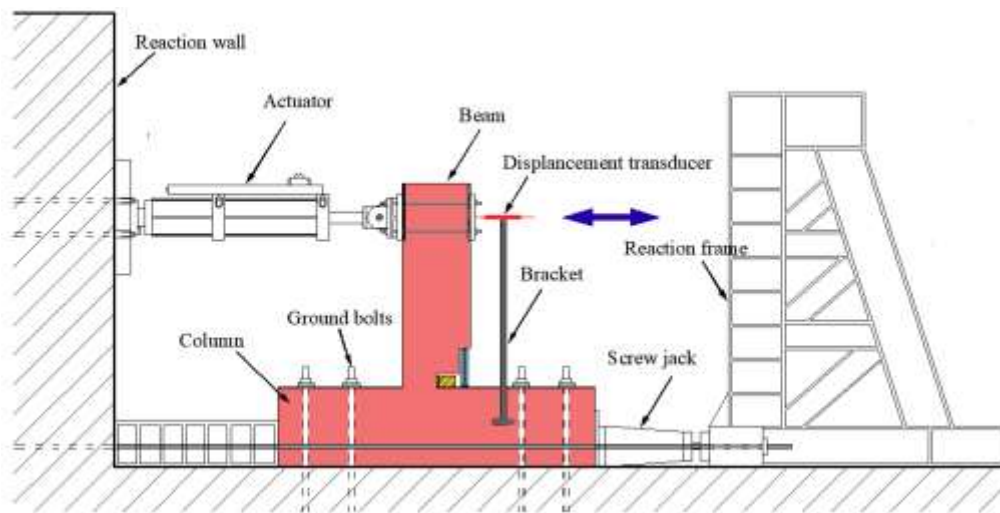
No.	Yielding strength f_y (MPa)	Ultimate strength f_p (MPa)	Young's modulus E_s (N/mm ²)	Yield ratio (%)	Ductility (%)
A	271.29	458.43	211468	59.18	38.51
B	262.31	456.30	214452	57.49	39.42
C	270.26	460.65	212122	58.67	39.55
Average	267.95	458.46	212681	58.45	39.16

11 3.3. Test setup and loading protocol

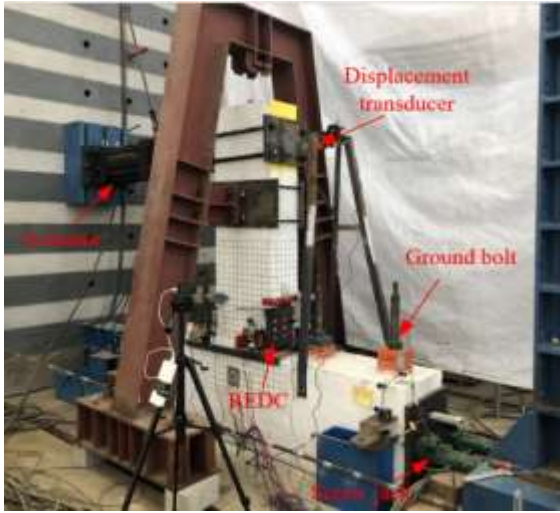
12 The beam–column assembly was rotated 90° for the test, and the test setup is shown in Fig.
 13 5. A lateral load was applied near the beam end using an actuator with a scale of ±1000 kN. A
 14 displacement transducer with a scale of ±150 mm was installed at the bottom of the beam to record

1 and calculate the relative rotation between the beam and the column during the tests. At the ends
2 of the column, two jacks were used to apply an axial load, which corresponded to an axial
3 compression ratio of 0.2, as recommended by the Code for Seismic Design of Buildings in China
4 (GB50010-2011) (2010), and restrict the horizontal movement of the assembly. Additionally, two
5 displacement transducers were placed at the same position to detect horizontal movement for
6 enhancing the accuracy of the measurements.

7 The drift sequence in Fig. 6 was adopted in accordance with the American Concrete Institute
8 (ACI) acceptance criteria for moment frames (ACI Committee 374, 2005). The test specimens
9 were subjected to three cycles at drift levels of 0.1%, 0.2%, 0.5%, 0.75%, 1.0%, 1.5%, 2.0%, 2.5%,
10 3.5%, and 4.5%. A smaller cycle—one-third of the previous drift—followed each large drift set
11 for closing the gaps between the aggregates in the concrete.



(a). Test setup and instrumentations



(b). Photograph of the specimen under test

Fig. 5 The specimen under test

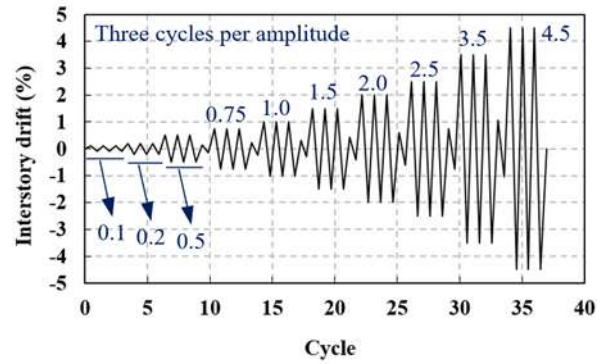


Fig. 6 Quasi-static loading

3.4. Test matrix

The thickness of the REDC core plate and the structural details of the REDC are significant design parameters that affect the hysteretic responses of this novel precast connection. To investigate the seismic behaviors in this novel precast connection, a specimen was subjected to three tests with variations in the design parameters. The design parameters used for the tests are presented in Table 4. In Test 1, the thickness of the REDC core plate was 12 mm, and the core plate contained no stoppers and unbonding material. Additionally, 4.8-grade M12 × 60 mm ordinary bolts were used to connect the REDC. In Test 2, the thickness of the REDC core plate was 10 mm, and the core plate contained no stoppers and unbonding material. Different from the Test 1, 10.9-grade M14 × 60 mm high-strength bolts were used to connect the REDC in Test 2. In Test 3, the thickness of the REDC core plate was 14 mm, and the connected bolts were 10.9-grade M14 × 60 mm high-strength bolts. Different from Tests 1 and 2, the core plate had stoppers (two 10-mm-long connections) and unbonding material in Test 3. The stopper in the Test 3 is used to

1 fix the restraining plates and the filler plates in the center of the core plate, so as to reduce the
 2 friction of the core plate and the restraining plates. At the same time, the unbonding material is
 3 used to reduce the friction between the core plate and the restraining plates. By reducing friction,
 4 the neck phenomenon of the core plate and the stress concentration will be reduced.

5 **Table 4** Test matrix

Test number	Thickness of the core plate (mm)	Bolt parameters		Stopper	Unbonding Material
		Type	Size (mm)		
Test 1	12	4.8-grade	M12 × 60	—	N
Test 2	10	10.9-grade	M14 × 60	—	N
Test 3	14	10.9-grade	M14 × 60	10 mm	Y

6
 7 **4. Experimental results and discussion**

8 **4.1. Hysteretic response**

9 The hysteretic responses of the three tests are shown in Fig. 7. In all the tests, failure occurred
 10 via the fracture of the REDC core plate owing to the low-cyclic fatigue. The drift ratios were
 11 calculated by dividing the displacement at the tip of the beam by the shear span (the shear span
 12 was 1500 mm). The drift ratio in the hysteretic response (Fig. 7) was the relative drift of the beam
 13 and column, which is measured by the displacement transducer fixed on the column (shows in
 14 Fig.5). Therefore, the drift ratio of the hysteresis response in Fig. 7 is authentic and fully shows
 15 the true hysteresis performance of this novel precast connection. It can be clearly seen that the drift
 16 ratio in the hysteretic curve is smaller than that in loading protocol, due to the gap between the
 17 actuator and the specimen and the slight slip in the loading process. In addition, as shown in Fig.
 18 7(a), the positive and negative drifts of Test 1 differed at the same loading level. At the same time,
 19 the negative drift in the Test 1 hysteretic curve (Fig. 7(a)) is smaller than the drift in the loading

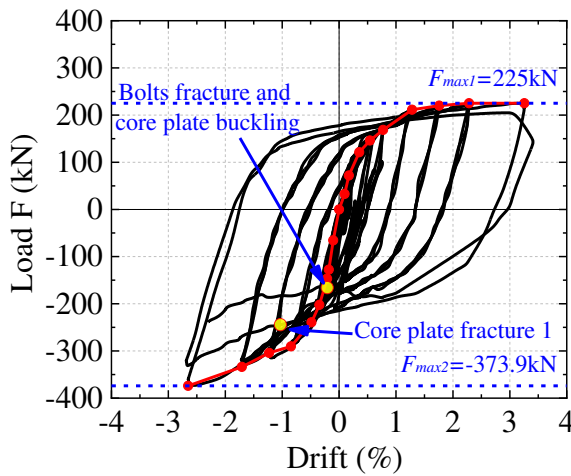
1 protocol. It is attributed the rigid-body rotation and slippage of the specimen in the negative drift
2 caused by anchor failure of the two ground bolts in the left side of the specimen. In order to avoid
3 this phenomenon happening again in the Test 2 and Test 3, two anchor failed ground bolts were
4 refastened after the Test 1, and a stronger torsional moment was applied to the ground bolts.

5 In the test 1, as shown in Fig. 7(a), the maximum positive drift sustained in Test 1 was 3.41%
6 (the corresponding drift level in the loading protocol was 3.5%), and the maximum positive force
7 was 225kN corresponding the first cycle at this level. The negative maximum drift was -2.69%
8 (the corresponding drift level in the loading protocol was -3.5%), and the maximum negative
9 forces was -373.9kN corresponding the first cycle at this level. One side of the REDC core plate
10 fractured at -1.03% drift (during the second -3.5% drift cycle corresponding to the loading
11 protocol). In addition, the REDC core plate buckled at -0.21% drift (during the third -3.5% drift
12 cycle corresponding to the loading protocol), because the ordinary bolts connected the restraining
13 plates and the filler plates were fractured.

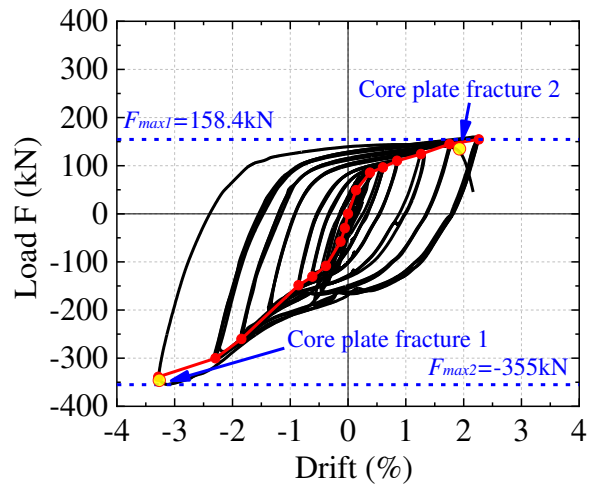
14 In the test 2, as shown in Fig. 7(b), the positive maximum drift sustained in Test 2 was 2.24%
15 (the corresponding drift level in the loading protocol was 2.5%), and the maximum positive force
16 was 158.4 kN corresponding the first cycle at this level. The negative maximum drift was -3.28%
17 (the corresponding drift level in the loading protocol was -3.5%), and the maximum negative force
18 was -355 kN corresponding the first cycle at this level. One side of the REDC core plate was
19 fractured when the loading drift increased to -3.27% (the corresponding drift level in the loading
20 protocol was the first -3.5% drift cycle), and the other side of the REDC core plate was fractured
21 when the loading drift increased to 1.93% (the corresponding drift level in the loading protocol

1 was the first 3.5% drift cycle).

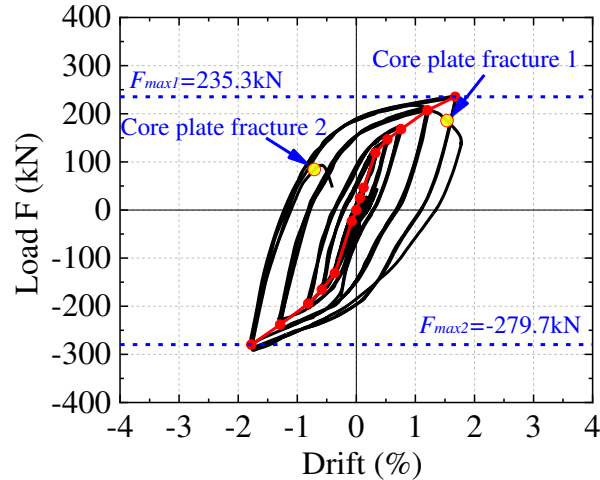
2 In the test 3, as shown in Fig. 7(c), the positive maximum drift sustained in Test 3 was 1.8%
3 (the corresponding drift level in the loading protocol was 2.0%), and the corresponding positive
4 maximum forces was 235.3 kN. The negative maximum drift was -1.81% (the corresponding drift
5 level in the loading protocol was -2.0%), and the corresponding negative maximum forces was -
6 279.7 kN. One side of the REDC core plate was fractured when the loading drift increased to -
7 1.54% (the corresponding drift level in the loading protocol was the third -2.0% drift cycle), and
8 the other side of the REDC core plate was fractured when the loading drift increased to -0.71%
9 (the corresponding drift level in the loading protocol was the fourth -2.0% drift cycle).



(a) Test 1 (12 mm)



(b) Test 2 (10 mm)



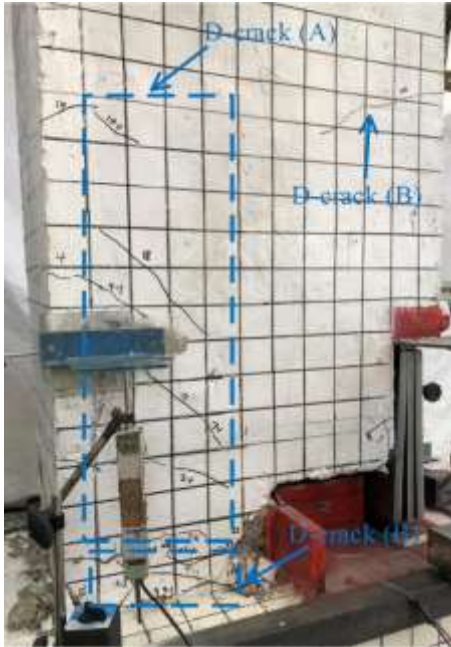
(c) Test 3 (14 mm)

Fig. 7 Load versus drift response for the SYPC connection: (a) Test 1; (b) Test 2; (c) Test 3

1 4.2. Cracking pattern

2 The cracking patterns of the front and back elevation in Tests 1 are shown in Figs. 8(a) and
 3 (b), respectively. Compared with Test 1, there were almost no new cracks in Test 2, and only a few
 4 of the original cracks continued to expand. It is attributed to the thickness of the core plate in Test
 5 2 is smaller than that in Test 1, so that the loading capacity of Test 2 is smaller than that in Test 1.
 6 In view of this, the cracking pattern in Test 2 is not presented. The cracking patterns of the front
 7 and back elevation in Tests 3 are shown in Figs. 8(c) and (d), respectively.

8 As shown in Fig. 8, the cracks were mainly concentrated in the top-hinge of the beam,
 9 including the shear cracks and the flexural cracks. The diagonal cracks were divided into two types:
 10 those under a positive drift (A) and those under a negative drift (B). As shown in Fig. 8, these two
 11 types of crack originated near the edge of the vertical slots and extended to the top reinforcements
 12 of the concrete beam at an angle of approximately 45°.



(a) Test 1 (front elevation)



(b) Test 1 (back elevation)



(c) Test 3 (front elevation)



(d) Test 3 (back elevation)

Fig. 8 Cracking patterns at the ultimate condition

- 1 In Test 1, the first crack occurred in the beam near the beam–column interface at a drift of 0.1%.
- 2 With an increase in the loading drift (to 0.2%, 0.5%, and 1.0%), flexural cracks under positive
- 3 loading developed in the upper part of the beam away from the beam–column interface.
- 4 Additionally, flexural cracks under negative loading developed in the lower part of the beam. Some

1 of the flexural cracks developed quickly at the top of the beam and connected with the cracks at
2 the back of the beam, forming through-cracks, which were the main cracks of the connections.
3 When the loading drift increased to 1.0% and 1.5%, shear cracks developed in the upper part of
4 the beam, which gradually developed from the upper part of the hidden corbel extending into the
5 plastic hinge zone. When the loading drift reached to -1.5% , the interface of the hidden corbel and
6 the beam was opened. When the drift increased further (to 2.0%, 2.5%, and 3.5%), the concrete
7 spalled in the upper part of the corbel and the top of the beam near the beam–column interface
8 owing to the compression damage. Because the bending capacity of the connection increased with
9 the increase of the thickness of the REDC in Test 3. New shear cracks and flexural cracks appear
10 in the larger loading drift. But the law of development is similar to Test 1.

11 **4.3.Failure mode**

12 As shown in Fig. 9(a), the fracture position of the REDC core plate in Test 1 was in the
13 yielding segment of the core plate, where one crack was formed. The REDC core plate were
14 fractured because of the large-strain, low-cycle fatigue. Because the unbonding material was not
15 used in Test 1, a necking phenomenon occurred in the REDC core plate, and several scratches
16 were clearly observed on the REDC core plate, which were caused by the friction between the core
17 plate and the restraint plate. The ordinary bolts (4.8-grade) connected the restraining plates and the
18 filler plates were fractured, as shown in Fig. 10(a). Two full waves were formed on the yielding
19 segment of the REDC core plate. Owing to the buckling of the REDC core plate, the waves
20 amplitudes of the REDC core plate in Test 1 were slightly large.



(a) Test 1 (12 mm)



(b) Test 2 (10 mm)



(c) Test 3 (14 mm)

Fig. 9 Failure pattern of the core plate



(a) Test 1 (12 mm)



(b) Test 2 (10 mm)



(c) Test 3 (14 mm)

Fig. 10 Buckling restraint state of the REDC

1 As shown in Fig. 9(b), because the unbonding material was not used in Test 2, necking
 2 occurred in the REDC core plate, and several scratches were clearly observed on the REDC core
 3 plate, which were caused by the friction between the core plate and the restraint plate. The fracture
 4 position of the REDC core plate in Test 2 was in the yielding segment of the core plate, where two
 5 cracks were formed. Because high-strength bolts were used in Test 2, the REDC core plate was

1 effectively protected from buckling by the restraint plates, as shown in Fig. 10(b).

2 As shown in Fig. 9(c), because of the stoppers and the unbonding material was used in Test
3 3, no scratches were clearly observed in the REDC core plate. The necking phenomenon was not
4 obvious in the REDC core plate. At the same time, the fracture position of the REDC core plate in
5 Test 3 was at the junction of the yielding segment and the transition segment. On the other side, a
6 crack were formed at the middle of the yielding segment of the core plate (near the stopper).
7 Combined with the phenomenon that the drift in Test 3 is relatively smaller than that in Tests 1 and
8 2, it can be attributed to the initial defect of the core plate caused by the wire electrical discharge
9 machining (WEDM) technology. In order to realize a 10mm stopper and a 1mm gap between the
10 core plate and the filling plate, WEDM technology was easily cause initial defect to the core plate.
11 This initial defect leaded to early failure of REDC, which limited the ductility of REDC. It can be
12 well proved by the phenomenon of no obvious necking in REDC core plate and its special failure
13 position. Because high-strength bolts (10.9-grade) were used in Test 3, the REDC core plate was
14 effectively protected from buckling by the restraint plates, as shown in Fig. 10(c).

15 **4.4. Energy dissipation**

16 The energy-dissipation capability is an important index for evaluating the seismic behavior
17 of structures. The energy dissipation per cycle was used to evaluate the energy dissipation of the
18 novel precast connection. The energy dissipation per cycle of the three tests corresponding to the
19 positive and negative drifts were examined. The energy dissipation of the smaller cycles and the
20 equivalent viscous damping ratio of the smaller cycles and the incomplete final cycles were
21 ignored. The energy dissipation per cycle is plotted in Figs. 11.

1 With the gap opening and closing, the energy dissipation per cycle of the novel precast
2 connection exhibited an almost symmetrical “V” shape, as shown in Fig. 10. In the three tests, the
3 energy dissipation per cycle was relatively small when the drift ratio was small ($<0.5\%$). However,
4 it increased significantly with the increase of the drift ratio. As indicated by Fig. 11, the energy
5 dissipation per cycle in Test 3 (under both the positive and negative drifts) was greater than that in
6 Test 1, and the energy dissipation per cycle in Test 1 was greater than that in Test 2. The results
7 suggest that the energy dissipation per cycle of the novel precast connection increased with the
8 thickness of the REDC core plate. Additionally, the difference in the energy dissipation per cycle
9 between Tests 2 and 1 was greater than that between Tests 3 and 2. This is because the energy-
10 dissipation capacity of the novel precast connection in Test 1 consisted of the energy-dissipation
11 capacity provided by concrete crushing between the beam–column surfaces and the energy-
12 dissipation capacity provided by the REDC. However, in Tests 2 and 3, the energy-dissipation
13 capacity of the novel precast connection was only provided by the REDC, because the plastic hinge
14 of the specimen was fully formed after Test 1. Finally, it can be seen from Fig. 11 that, at the same
15 load level, the energy dissipation values per cycle under positive and negative displacement ratios
16 are approximate, indicating that the energy dissipation capacity of the novel precast connection is
17 good under both positive and negative bending moments.

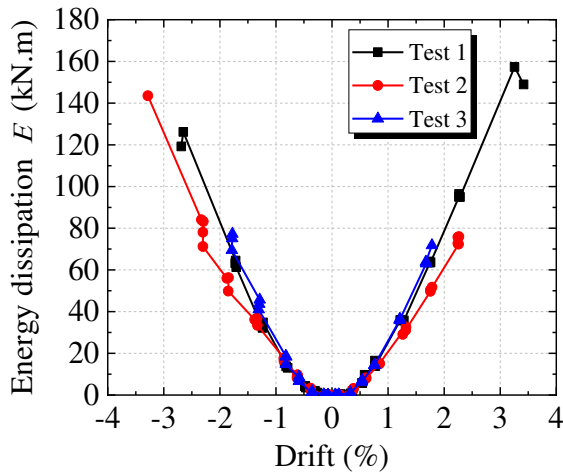


Fig. 11 Energy dissipation per cycle versus drift ratio.

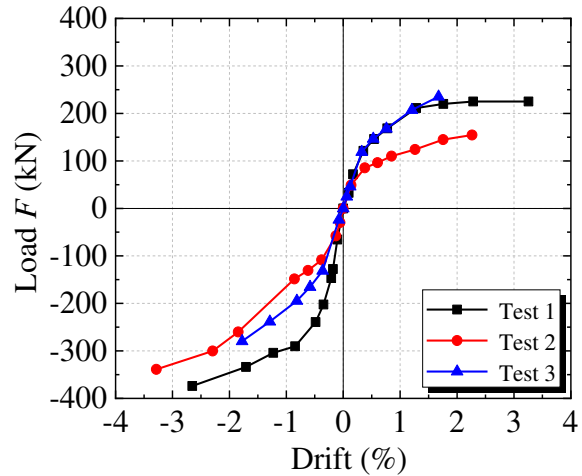


Fig. 12 Skeleton curve

1 4.5.Skeleton curve

2 The skeleton curves of the three tests are presented in Fig. 12. As shown in Fig. 12, the
 3 negative force was greater than the positive force at the same drift, and the discrepancy was more
 4 significant in Tests 1 and 2 than in Test 3. Although the thickness of REDC core plate in Test 1 is
 5 less than that in Test 3. However, the positive force of test 3 is very close to that of test 1 at the
 6 same positive drift. This is attributed to the contribution of the concrete compression zone in Test
 7 1. In addition, the positive force in Test 1 was greater than that in Test 2. The results are attributed
 8 to the differences in the thickness of the REDC core plate. At the same time, in Tests 2 and 3, the
 9 plastic hinge was completely formed, and the concrete compression zone no longer provided
 10 compressive stress. It can be concluded that the load capacity of the novel precast connection is
 11 directly influenced by the parameters of the REDC.

12 Additionally, at the same negative drift, the negative force in Test 1 was greater than that in
 13 Test 2, and the negative force in Test 2 was greater than that in Test 3. In addition, the difference
 14 in the negative force between Tests 1 and 2 was greater than that the difference in the negative

1 force between Tests 2 and 3. This is most likely because the compressive stress provided by the
2 concrete compression zone made the top reinforcements yield at the initial loading process, then
3 the load-bearing capacity of the connection increased rapidly. As mentioned previously, the plastic
4 hinge was completely formed in Test 1. The concrete compression zone no longer provided
5 compressive stress in Tests 2 and 3. Another important reason is that the yield stress of the top
6 reinforcements was increased by the “cold drawing” effect after the loading in Test 1, which
7 delayed the yielding of the top reinforcements compared with that in Test 1. The “cold drawing”
8 effect means that the yield stress and strain of the reinforcement after a tensile yield is increased
9 compared with the initial state. Additionally, the thickness of the REDC core plate in Test 2
10 decreased, making the load capacity in Test 2 lower than that in Test 1. In Test 3, because twice
11 “cold drawing” effect in Tests 1 and 2, the yield stress of the top reinforcements was further
12 increased. Combined with the reason of the fully developed plastic hinge, the load capacity in Test
13 3 was lower than that in Test 1, although the thickness of the core plate increased.

14 **4.6.Top longitudinal reinforcement strain profile**

15 Because three tests were successively performed on a single novel precast connection
16 specimen, the top longitudinal reinforcement strain in Test 1 was the key to the study. Fig. 13
17 presents the top longitudinal reinforcement strain profile and the strain history of the top
18 reinforcement at the column face for Test 1. Fig. 13(a) and (a) show the peak strain of the top
19 longitudinal reinforcements corresponding to each peak positive and negative drift, respectively.
20 Additionally, the actual peak drift of each cycle is shown in the figure legend, and the
21 corresponding drift in the loading protocol is shown in brackets.

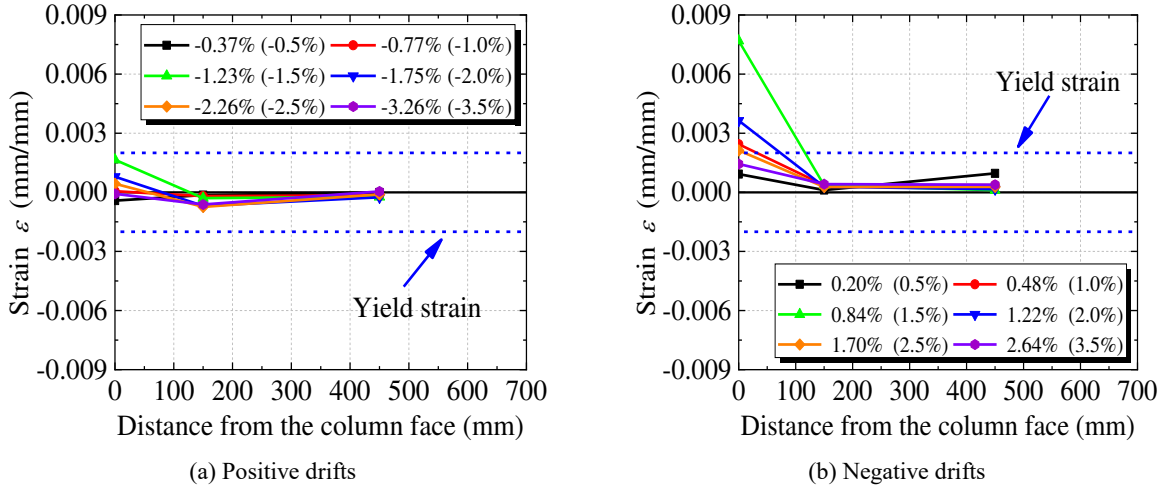


Fig. 13 Strain profiles of the top reinforcement in Test 1

1 As shown in Fig. 13, the variation of the top reinforcement strain was the largest at 0 mm
 2 from the column face, and the reinforcements yielded. The top reinforcement strains at 150 and
 3 450 mm were small and always remained elastic. The top reinforcement yielded under the positive
 4 drift (Fig. 13(b)), whereas they were always elastic under the positive drift (Fig. 13(a)). In addition,
 5 some tensile strains during gap-opening rotations exhibited when compression would be expected.
 6 This is most likely the result of larger residual tensile strains, from previous gap-closing cycles,
 7 allowing compressive stresses to occur at positive strains.

8 Eqs. (5) and (6) are force balance formulas of the connection. After expansion and
 9 transformation, Eqs. (7) and (8) can be obtained:

$$T'_s = C'_s + C_{c, \text{ bottom}} \quad (5)$$

$$T_s = C'_s + C_{c, \text{ top}} \quad (6)$$

$$A'_s f'_s = A_s f_y + a_l f'_c \beta (d_c - c) b \quad (7)$$

$$A_s f_y = A'_s f'_s + a_l f'_c \beta c b \quad (8)$$

10 With the increase of the negative drift, the compression of the REDC (C_s) and the concrete

1 compression zone ($C_{c, \text{bottom}}$) both increased continuously (Eq. (5)). Although the $A'_s f'_y / A_s f_y$ is 3.68
2 (>2.5) in the specimen, the compression force provided by the concrete compression zone ($C_{c, \text{bottom}}$)
3 is very larger. Therefore the tensile stress of the top longitudinal reinforcements quickly
4 increased until the top reinforcements yielded. Under the positive drift, the compression (C'_s)
5 provided by the top longitudinal reinforcements and the compression ($C_{c, \text{top}}$) provided by the
6 concrete compression zone worked together to counteract the tension (T_s) provided by the REDC,
7 as shown in Eq. (6). Owing to the limited strain-hardening of the REDC core plate and the
8 $A'_s f'_y / A_s f_y$ is 3.68 (>2.5), the top reinforcements remained elastic at all positive drift.

9 **4.7. Additional bending moment**

10 The additional bending moment is an important cause of connection damage. The additional
11 bending moment of the connection is also a major obstacle to the formation of the "strong column
12 and weak beam" mechanism, which also brings troubles to the design. Therefore, this novel precast
13 connection research tries to control the bending moment of the connection by reducing the
14 additional bending moment.

15 The bending moment of the conventional beam-column connection is produced by the
16 combined action of the pressure generated by the concrete compression zone and the top/bottom
17 reinforcements and the tension generated by the bottom/top reinforcements. If the top and bottom
18 reinforcements in beam is the same, the positive and negative bending moments are as shown in
19 Eq. (9). Then the additional bending moment ($M_{\text{additional}}$) produced by the combined action of the
20 pressure generated by the concrete compression zone and the tension generated by the top/bottom
21 reinforcements can be expressed by Eq.(10).

$$M_n^{\pm} = A_s f_y (d-d') + a_1 f'_c \beta (d-c) b (d-a/2) \quad (9)$$

$$M_{\text{additional}} = a_1 f'_c \beta (d-c) b (d-a/2) \quad (10)$$

1 The novel beam-column connection proposed in this paper attempts to reduce the height of
 2 the concrete compression zone through vertical slot, thereby reducing $M_{\text{additional}}$. In addition to the
 3 vertical slot, increasing $A'_s f'_y / A_s f_y$ is used to reduce the strain of the top reinforcements. Through
 4 this structural form, the positive and negative bending moment of the novel beam-column
 5 connection strive to be governed by the yielding of the REDC. So as to realize the design goal of
 6 controllable bending moment of the connection.

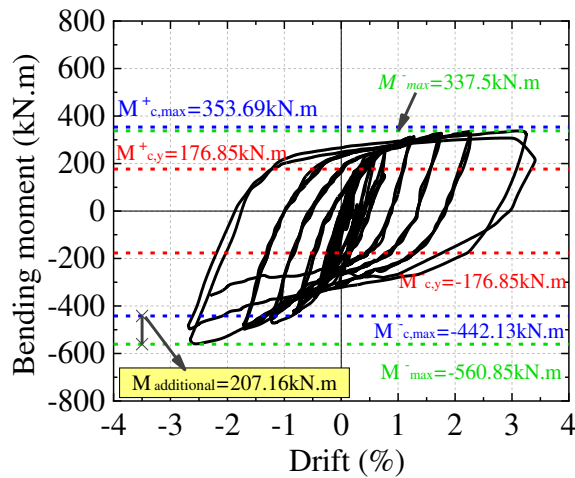


Fig. 14 Schematic diagram of additional bending moment.

7 Fig.14 is an illustration of the $M_{\text{additional}}$ discussion with an example of Test 1. $M_{c,y}^+$ and $M_{c,y}^-$
 8 are the positive and negative yield bending moment calculated by multiplying the yield force of
 9 the REDC about a lever arm. They can be called the controllable yield bending moment, as shown
 10 in Eqs. (11) and (12). $M_{c,max}^+$ and $M_{c,max}^-$ are the overstrength bending moment (considering strain
 11 hardening of REDC) of the REDC calculated by multiplying the $M_{c,y}^+$ and $M_{c,y}^-$ about a
 12 overstrength factor as shown in Eqs. (13) and (14), which can be called the maximum controllable

1 bending moment. The overstrength coefficient of REDC under tension is conservatively taken as
 2 2.0. Considering that the REDC is essentially a BRB, when the BRB is compressed, due to the
 3 friction between the core plate and the restraining plate, the compression force of the REDC will
 4 be higher than the tension force. Therefore, the overstrength coefficient of REDC under
 5 compression is conservatively taken as 2.5. When $M_{\text{additional}}$ is zero, the height of the vertical slot
 6 in the connection is close to the $d=h-(d'+1/2d_{\text{reinforcemet}})$, where h represents the height of beam,
 7 $d_{\text{reinforcemet}}$ represents the diameter of the top longitudinal reinforcement. In this case, it can be
 8 approximately considered that under the positive bending moment, the resultant of the concrete
 9 compression zone near the center of the reinforcements. Therefore, $a/2$ in Eqs. (11) and (13) can
 10 be approximately replaced by d' .

$$M_{c,y}^+ = A_s f_y (d-a/2) \quad (11)$$

$$M_{c,y}^- = A_s f_y (d-d') \quad (12)$$

$$M_{c,\max}^+ = A_s f_y \times 2 \times (d-a/2) \quad (13)$$

$$M_{c,\max}^- = A_s f_y \times 2.5 \times (d-d') \quad (14)$$

11 It can be seen from Fig.14 that the maximum bending moment M_{\max}^+ is very close to the
 12 maximum controllable bending moment $M_{c,\max}^+$ of the novel beam-column connection. This
 13 shows that the positive bending moment of the novel beam-column connection proposed in this
 14 paper is governed by the yielding of the REDC. In other words, the positive bending moment of
 15 the novel beam-column connection is controllable. In addition, the negative maximum bending
 16 moment M_{\max}^- of the novel beam-column connection is larger than the maximum controllable
 17 bending moment $M_{c,\max}^-$. It is obvious that the extra part is $M_{\text{additional}}$. It shows that the negative

1 bending moment of the novel beam-column connection is not completely governed by the yielding
2 of the REDC, and extra part is controlled by the compression force generated by the concrete
3 compression zone. This can also be clearly seen from the Eq. (2). However, it is worth mentioning
4 that the negative bending moment of novel beam-column connection is smaller than that of the
5 conventional beam-column connection. The $M_{\text{additional, novel}}$ of the novel beam-column connection
6 proposed in this paper can be expressed by Eq. (15):

$$M_{\text{additional, novel}} = a_1 f'_c \beta (d_c - c) b (d_c - a/2) \quad (15)$$

7 Compared with Eq. (10), because the height of the vertical slot is the half of the beam height.
8 Therefore, the $M_{\text{additional, novel}}$ of the novel beam-column connection is significantly smaller than
9 $M_{\text{additional}}$ of the conventional beam-column connection.

10 **5. Decrease top longitudinal reinforcement strain and additional bending moment under** 11 **positive drift**

12 Au (2010) proposed that for the top reinforcement to remain elastic, $A'_s f'_y / A_s f_y$ must be >2.5 .
13 Therefore, the $A'_s f'_y / A_s f_y$ of this novel precast connection test specimen was 3.68 (>2.5). However,
14 during the loading process, the top longitudinal reinforcements still yielded. According to the
15 theory analysis in Section 4.6 and 4.7, a method is proposed to decrease top longitudinal
16 reinforcement strain and additional bending moment under positive drift by increasing the height
17 of the slot (decrease the height of the concrete compression zone). At same time, the method is
18 verified by finite-element simulations.

19 Numerical analyses were performed using ABAQUS, as shown in Fig. 15. The concrete, steel
20 corbel, and REDC were modelled by eight-node three-dimensional (3D) linear brick elements with

1 reduced integration (C3D8R), and the reinforcements were modelled by two-node 3D linear truss
2 elements (T3D2). The reinforcements were embedded in the concrete. The surface-to-surface
3 hard contact interaction was applied to the interface between the steel corbel and the precast beam,
4 and the friction coefficient was assumed to be 0.35. The damage plasticity model for concrete in
5 ABAQUS was utilized to simulate the concrete. A bilinear kinematic hardening model considering
6 the stiffness degradation of steel was used to simulate the steel corbels, reinforcements, and REDC.
7 All the parameters in this model were set according to the material test results (Tables.1-3). All the
8 geometric dimensions of the model were identical to those of the test specimen. The boundary
9 conditions of the connection in the model were identical to those in the test. The depths of the top
10 hinge in the three models were 300 mm ($d_c/d = 1/2$), 200 mm ($d_c/d = 1/3$), and 100 mm ($d_c/d =$
11 $1/6$). To simplify the model and identify the factors influencing the top longitudinal reinforcement
12 strain, a pushover analysis was performed on each model. It was assumed that the REDC would
13 not fail, i.e., could still function, at a drift ratio of 3%.

14 The Fig. 16 compares the response of the 300mm analytical model with the experimental
15 response of the Test1. Because the finite element model is a pushover analysis, the finite element
16 simulation is compared with the skeleton curve. It shows that the element is capable of accurately
17 modelling the global force-drift response of the subassembly.

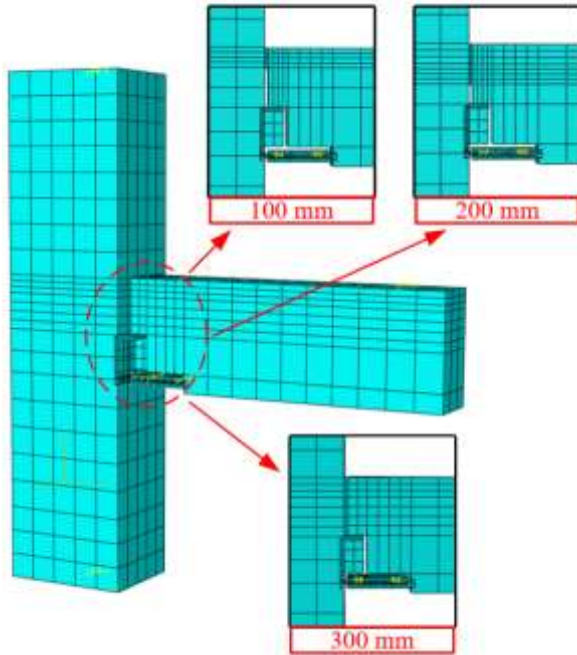


Fig. 15 ABAQUS model for the novel precast connection

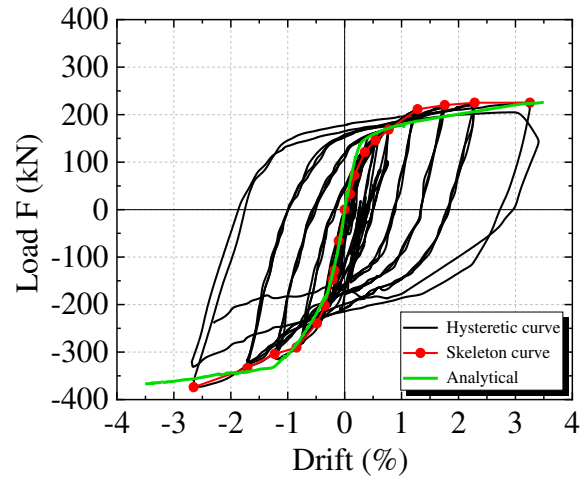
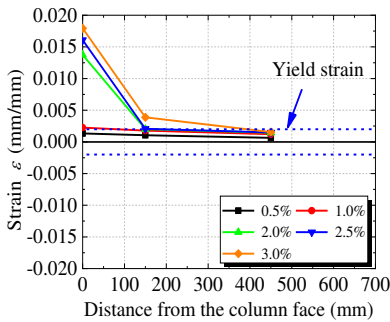
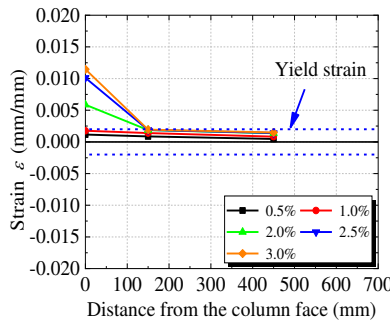


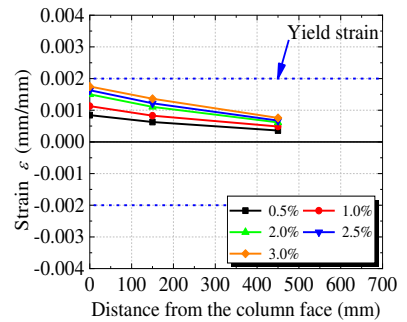
Fig. 16 Comparison of analytical and experimental results



(a) Strain profile in top reinforcement at the negative peak drifts (300 mm)



(b) Strain profile in top reinforcement at the negative peak drifts (200 mm)



(c) Strain profile in top reinforcement at the negative peak drifts (100 mm)

Fig. 17 The peak strain of the top longitudinal reinforcement corresponding to each positive peak drift in the three models.

1 The strain of the top longitudinal reinforcement corresponding to negative drifts is the focus
 2 of research. The strain of the top longitudinal reinforcements corresponding to each negative peak
 3 drift in the three models is presented in Fig. 17. The strain profiles of the top longitudinal
 4 reinforcement in three models were similar to the test result. The variation of the top reinforcement
 5 strain was the largest at 0 mm from the column face. The variations of the top reinforcement strains
 6 at 150 and 450 mm were relatively small. By comparing Fig. 17 (a) - (c), it can be found that the

1 top reinforcement decreases with the increase of the slot height (the decrease of the top hinge
2 depth). In the model with slot height of 500mm (top hinge depth of 100mm), the strain of top
3 reinforcement corresponding to negative drifts remains elastic. As shown in Figs. 17(a)–(c), with
4 the decrease of the top-hinge depth (the increase of the vertical slot height), the top longitudinal
5 reinforcement strain decreased significantly. When the top-hinge depth was 100 mm ($d_c/d = 1/6$),
6 the top reinforcement always remained elastic. However, this was smaller than the value of $d_c/d =$
7 $1/4$ recommended by Au (2010). Fig. 18 is the comparison of the bending moment of the three
8 models. It can be clearly seen that the negative bending moment of the connection decreases with
9 the increase of the vertical slot height (decrease of the top-hinge depth). When the top-hinge depth
10 is 100mm (vertical slot height is 500mm), the negative maximum bending moment $M_{c,max}^-$ is close
11 to the negative maximum controllable bending moment $M_{c,max}^-$. This well confirmed that when
12 the vertical slot height increased to a certain value, the positive and negative bending moment of
13 the novel connection is controllable. In other words, at this time, the positive and negative bending
14 moment of the novel beam-column connection can be governed by the yielding of the REDC.

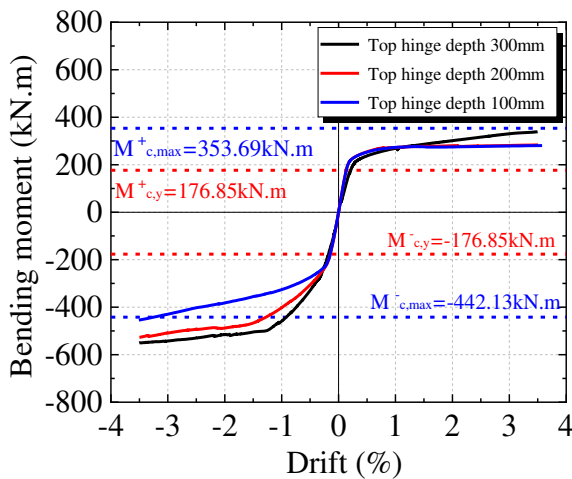


Fig. 18 The comparison of the bending moment

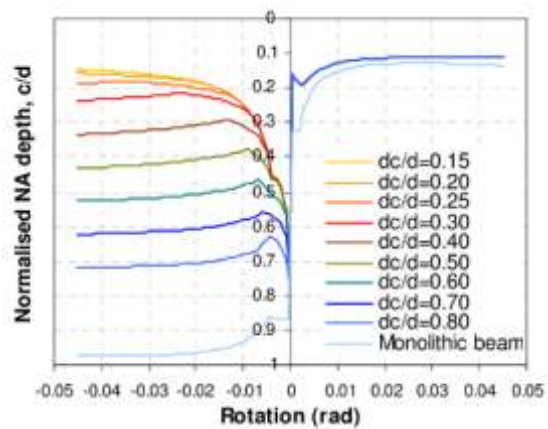


Fig. 19 Parametric study for the concrete top-hinge depth (Au

6. Recommended design value of the top hinge depth

To obtain the recommended design value, further theoretical analysis of the finite-element model is needed. The neutral-axis depth is affected by the height of the vertical slot. When the top-hinge depth decreased sufficiently, the neutral axis was infinitely close to the top longitudinal reinforcement of the novel precast connection. According to the force-balance relationship, the position of the neutral axis must be below the top longitudinal reinforcement. As shown in Fig. 19, when the top-hinge depth varied from $0.15d$ to $0.3d$, the position of the neutral axis was close to the top longitudinal reinforcement. Thus, the height of the concrete compression zone ($d_c - c$) was close to the height of the concrete below the top longitudinal reinforcement in the top hinge ($d' - 1/2d_{\text{reinforcement}}$), where $d_{\text{reinforcement}}$ represents the diameter of the top longitudinal reinforcement. Therefore, in determining the height of the concrete compression zone and developing a formula for calculating the height of the beam hinge, it is conservative to consider that the neutral-axis position is the position of the lower edge of the top longitudinal reinforcement. When the material properties and geometric dimensions of the connection are known, the safe (maximum) top-hinge depth for ensuring that the top longitudinal reinforcement remains elastic can be calculated as follows:

$$d_c = (A'_s f'_s - A_s f_s) / (\alpha_1 f'_c \beta b) + c \quad (16)$$

According to this assumption, c was the distance from the lower edge of the top longitudinal reinforcement to the top surface of the beam, i.e., $(d' + 1/2d_{\text{reinforcement}})$. When the top-hinge depth is less than or equal to the d_c obtained via Eq. (16), the top longitudinal reinforcement does not yield.

1 Considering the increase of the concrete compression stress due to the constraint influence of
 2 stirrups, the amplification coefficient ϕ is introduced in Eq. (16). J. B. Mander et al. (1988)
 3 proposed the compressive strength of confined concrete can be calculated as follows:

$$f'_{cc} = f'_{co} \left(-1.254 + 2.254 \sqrt{1 + \frac{7.94f'_1}{f'_{co}}} - 2 \frac{f'_1}{f'_{co}} \right) \quad (17)$$

4 Therefore, ϕ can be calculated as follows:

$$\phi = -1.254 + 2.254 \sqrt{1 + \frac{7.94f'_1}{f'_{co}}} - 2 \frac{f'_1}{f'_{co}} \quad (18)$$

5 Where f'_{co} is the unconfined concrete compressive strength; and f'_1 is the effective lateral confining
 6 stress on the concrete. In order to simplify the calculation, it is approximately specified in this
 7 paper that $\phi = 1.65$.

8 According to the material properties and geometric dimensions of the connection of the
 9 specimen, the safe top-hinge depth for ensuring that the top longitudinal reinforcement remains
 10 elastic is 102.75 mm, smaller than the value of $1/4d = 150$ mm proposed by Au (2010). Compared
 11 with the constant value of $1/4d$, the d_c obtained via Eq. (16) is influenced by various parameters.
 12 Therefore, the top-hinge depth obtained using Eq. (16) is more reasonable, accurate, and safe.

13 **7. Conclusion**

14 To realize the controllable bending moment of connections and the principle of “strong
 15 column weak beam”, a novel precast connection was proposed. According to a theoretical analysis,
 16 experimental research, and numerical simulations, the structural form, stress mechanism, and
 17 seismic performance of the connection were investigated in detail, and relevant design suggestions
 18 were provided. The following conclusions are drawn:

- 1 (1) The novel precast connection has the characteristics of a simple structure and easy
2 construction. The REDC is placed at the same horizontal position as the bottom longitudinal
3 reinforcement. The steel corbel is embedded in the column and arranged at the half-height of
4 the beam to effectively transfer the vertical shear force. A vertical slot is installed at the bottom
5 of the beam, adjacent to the column face. According to the Damage Avoidance Design (DAD)
6 approach, the damage of the novel precast connection is mainly concentrated in REDC. After
7 the earthquake, the structures can be repaired quickly by replacing the REDCs.
- 8 (2) The force-transfer mechanism of the novel precast connection is direct. Under a positive drift
9 (gap opening), the moment transfer mechanism and shear transfer mechanism are similar to
10 those of the conventional concrete beam–column connection. Under a negative drift (gap
11 closing), owing to the vertical slot, compared with the conventional concrete beam–column
12 connection, the compression force provided by the concrete compression zone in the novel
13 precast connection has been reduced. For the positive drift (gap opening), the shear is
14 transferred primarily via the concrete compression zone. For the negative drift (gap closing),
15 the shear is carried primarily by the steel corbel.
- 16 (3) The seismic performance of the novel precast connection is excellent, particularly the energy-
17 dissipation capacity and load capacity. The energy-dissipation capacity and load capacity are
18 directly influenced by the REDC. When the thickness of the REDC core plate increased within
19 a reasonable range, the energy-dissipation capacity and bearing capacity of the novel precast
20 connection can be improved.
- 21 (4) By reducing the top-hinge depth (increasing the height of the vertical slot), the top longitudinal

1 reinforcement can be kept in the elastic. At the same time, the designs goal of a “controllable
2 flexural bearing capacity” (reduce the additional bending moment governed by the
3 compression of the concrete compression zone) and the principle of “strong column weak beam”
4 can be realized.

5 (5) A design method and calculation formula for reducing the additional bending moment are
6 proposed. It can provide the design basis for realizing the characteristic of the controllable
7 bending moment. At the same time, this index can be calculated more accurately according to
8 this formula.

10 **Acknowledgments**

11 The authors would like to acknowledge financial supports from the China National Key
12 Research and Development Program (2019YFC1509305), the National Natural Science
13 Foundation (51978165).

15 **Reference**

16 Amaris A, Pampanin S, Bull D K, Carr A (2008) Experimental investigation on a hybrid jointed
17 precast frame with non-tearing floor connections. In: New Zealand Society for Earthquake
18 Engineering Conference, New Zealand.

19 ASCE/SEI 41-06. (2007) Seismic Rehabilitation of Existing Buildings Published by the American
20 Society of Civil Engineers (ASCE), Prepared by the Structural Engineering Institute of ASCE.

21 Au, E. V. (2010) The mechanics and design of a non-tearing floor connection using slotted

- 1 reinforced concrete beams. Master Dissertation, University of Canterbury, Christchurch, New
2 Zealand.
- 3 Bacht T, Chase J G, MacRae G, et al. (2011) HF2V dissipator effects on the performance of a 3
4 story moment frame. *Journal of Constructional Steel Research* 67(12): 1843-1849.
- 5 Blakeley, Roger W. G., and R. Park. (1971) Seismic Resistance of Prestressed Concrete Beam-
6 Column Assemblies. *ACI Structural Journal* 68(9): 677-692.
- 7 Bull D K. (2003) Understanding the Complexities of Designing Diaphragms in Buildings for
8 Earthquakes. In: *Symposium to Celebrate the Lifetime Contributions of Tom Paulay and Bob*
9 *Park, Christchurch, New Zealand.*
- 10 C. A. Muir, D. K. Bull, and S. Pampanin. (2013) Seismic testing of the slotted beam detail for
11 reinforced concrete structures. *Proceedings of the 2013 Structures Congress* 2614-2625.
- 12 Chanchi Golondrino, Jose Christian , et al. (2018) Asymmetrical friction connections post-heating
13 behavior. *Journal of Constructional Steel Research* 149(OCT.): 119-129.
- 14 Chanchi Golondrino, Jose Christian , et al. (2019) Asymmetric Friction Connection (AFC) design
15 for seismic energy dissipation. *Journal of Constructional Steel Research* 157(JUN.): 70-81.
- 16 Chang B, Hutchinson T, Wang X, Englekirk R. (2014) Seismic performance of beam-column
17 subassemblies with high-strength steel reinforcement. *ACI Structural Journal* 111(6): 1329.
- 18 Chang B, Hutchinson T C, Wang X, Englekirk R. (2012) Experimental seismic performance of
19 beam-column subassemblies using ductile embeds. *Journal of Structural Engineering* 139(9):
20 1555-1566.
- 21 Chi H, Liu J. (2012) Seismic behavior of post-tensioned column base for steel self-centering

1 moment resisting frame. *Journal of Constructional Steel Research* 78: 117-130.

2 Englekirk, R E. (1995) Development and testing of a ductile connector for assembling precast
3 concrete beams and columns. *PCI Journal* 40 (2): 36-50.

4 Englekirk, R E. (1996) An innovative design solution for precast prestressed concrete buildings in
5 high seismic zones. *PCI Journal* 41(4): 44-53.

6 Englekirk, R E. (2002) Design-construction of the paramount – a 39-story precast prestressed
7 concrete apartment building. *PCI Journal* 47 (4): 56-71.

8 Fan Li., Lv Xilin, Zhao Bin. (2007) Summary of Investigation on Seismic Behavior of Precast
9 Concrete Frame Structures. *Structural Engineer* 23(4): 90-97. (in Chinese)

10 Fenwick R C, Davidson B J. (1995) Elongation in ductile seismic-resistant reinforced concrete
11 frames. *Recent Developments in Lateral Force Transfer in Buildings, ACI SP-157*: 143-170.

12 Huang X, Eatherton M R, Zhou Z. (2020) Initial stiffness of self-centering systems and application
13 to self-centering-beam moment-frames. *Engineering Structures* 203: 109890.

14 Hassoun, M. N., and Al-Manaseer, A. (2020) *Structural Concrete: Theory and Design*. John Wiley
15 & sons.

16 Huang X, Zhou Z, Xie Q, et al. (2017) Force distribution analysis of self-centering coupled-beams
17 for moment-resisting-frames without floor elongation. *Engineering Structures* 147: 328-344

18 GB50011-2010. (2010) *Code for Seismic Design of Buildings (National Standards of the People’s*
19 *s Republic of China)*. Ministry of Construction of the People’s Republic of China. (in Chinese)

20 J.D.R. Byrne, Bull. D K. (2012) Design and testing of reinforced concrete frames incorporating
21 the slotted beam detail. In: *New Zealand Society for Earthquake Engineering Conference*,

- 1 Christchurch, New Zealand.
- 2 Kenyon E M. (2008) Predicting the seismic behavior of the Dywidag Ductile Connector (DDC)
3 precast concrete system. Master Dissertation, California Polytechnic State University, San
4 Luis Obispo, United States.
- 5 Köken A, Köroğlu M A. (2013) Experimental study on beam-to-column connections of steel frame
6 structures with steel slit dampers. *Journal of Performance of Constructed Facilities*, 2013,
7 29(2): 04014066.
- 8 Li C, Wu J, Zhang J, et al. (2020) Experimental study on seismic performance of precast concrete
9 frame with replaceable energy-dissipating connectors. *Engineering Structures*, 231: 111719.
- 10 Liu H, Yan Q., Du X. (2017) Seismic performance comparison between precast beam joints and
11 cast-in-place beam joints. *Advances in Structural Engineering* 20 (9): 1299-1314.
- 12 Linjie Huang, Zhen Zhou, Hao Liu, Yi Si. (2020) Experimental Investigation of Hysteretic
13 Performance of Self-Centering Glulam Beam-to-Column Joint with Friction Dampers.
14 *Journal of Earthquake and Tsunami* DOI: 10.1142/S1793431121500056.
- 15 Mander J B, Cheng C-T. (1997) Seismic resistance of bridge piers based on damage avoidance
16 design. Technical Report NCEER-97-0014 State University of New York at Buffalo, Buffalo,
17 USA: U.S. National Center for Earthquake Engineering Research (NCEER), Department of
18 Civil and Environmental Engineering.
- 19 Mander, J. B., Priestley, M. J., & Park, R. (1988) Theoretical stress-strain model for confined
20 concrete. *Journal of structural engineering*, 114(8), 1804-1826.
- 21 Mander T J, Rodgers G W, Chase J G, et al. (2009) Damage avoidance design steel beam-column

- 1 moment connection using high-force-to-volume dissipators. Journal of structural engineering
2 135(11): 1390-1397.
- 3 Marriott D. (2009) The development of high-performance post-tensioned rocking systems for the
4 seismic design of structures. Ph.D. Dissertation, University of Canterbury, Christchurch, New
5 Zealand.
- 6 Nakaki S D., Englekirk R E, Plaehn J L. (1994) Ductile connectors for a precast concrete frame.
7 PCI Journal 39(5): 46-59.
- 8 Ohkubo M, Hamamoto T. (2004) Developing reinforced concrete slotted beam structures to reduce
9 earthquake damage and to enhance seismic structural performance. In: 13th World
10 Conference on Earthquake Engineering. Vancouver, B.C, Canada.
- 11 Ohkubo M, Matsuoka T, Yoshioka T, Anderson D L. (2009) Shear transfer mechanism of
12 reinforced concrete beams with a slot at the beam-end. Proceedings of Japan Concrete
13 Institute 21(3), 301-306.
- 14 Oh S H, Kim Y J, Ryu H S. (2009) Seismic performance of steel structures with slit dampers.
15 Engineering Structures 31(9): 1997-2008.
- 16 Oudah F, El-Hacha R. (2013) Seismic performance of modified single-slotted beam concrete
17 connection. Journal of Earthquake Engineering 21(5):726-751.
- 18 Peng B H H, Dhakal R P, Fenwick R C, Carr A J. (2009) Modelling of RC moment resisting frames
19 with precast-prestressed flooring system. In: the 2009 New Zealand Society for Earthquake
20 Engineering, Christchurch, New Zealand, April.
- 21 Priestley, M J Nigel., and Macrae G A. (1996) Seismic tests of precast beam-to-column joint

- 1 subassemblages with unbonded tendons. PCI Journal 41(1): 64-81.
- 2 Priestley, M J Nigel. (1991) Overview of PRESSS Research Program. PCI Journal (4): 50-57.
- 3 Priestley, M J Nigel. (1996) The PRESSS Program-Current Status and Proposed Plans for Phase
4 III. PCI Journal (2): 22-40.
- 5 Rodgers G W. (2009) Next generation structural technologies: Implementing high force-to-volume
6 energy absorbers. Ph.D. Dissertation, University of Canterbury, Christchurch, New Zealand.
- 7 Thomphon K J. (1975) Ductility of concrete frames under seismic loading. Ph.D. Dissertation,
8 Department of Civil Engineering, University of Canterbury, New Zealand.
- 9 Tong C, Wu J, Hua K, Xie L. (2020) Low-Cycle Fatigue Life Estimation Curve for Buckling-
10 Restrained Braces Based on Cumulative Plastic Deformation. Journal of Earthquake
11 Engineering DOI: 10.1080/13632469.2020.1772152.
- 12 Tsutomu Usami, Chunlin Wang, Jyunki Funayama. (2011) Low-cycle fatigue tests of a type of
13 buckling-restrained braces. Procedia Engineering 14: 956-964.
- 14 Vasconez R M., Naaman A E, Wight J K. (1998) Behavior of HPFRC Connections for Precast
15 Concrete Frames Under Reversed Cyclic Loading. PCI Journal 43(6): 58-71.
- 16 Xie Luqi. (2020) Research on the mechanism of replaceable energy dissipation connector and its
17 seismic performance in precast concrete frame joint. Ph.D. Dissertation, Southeast University
18 (China), Nanjing, China. (in Chinese)
- 19

Figures

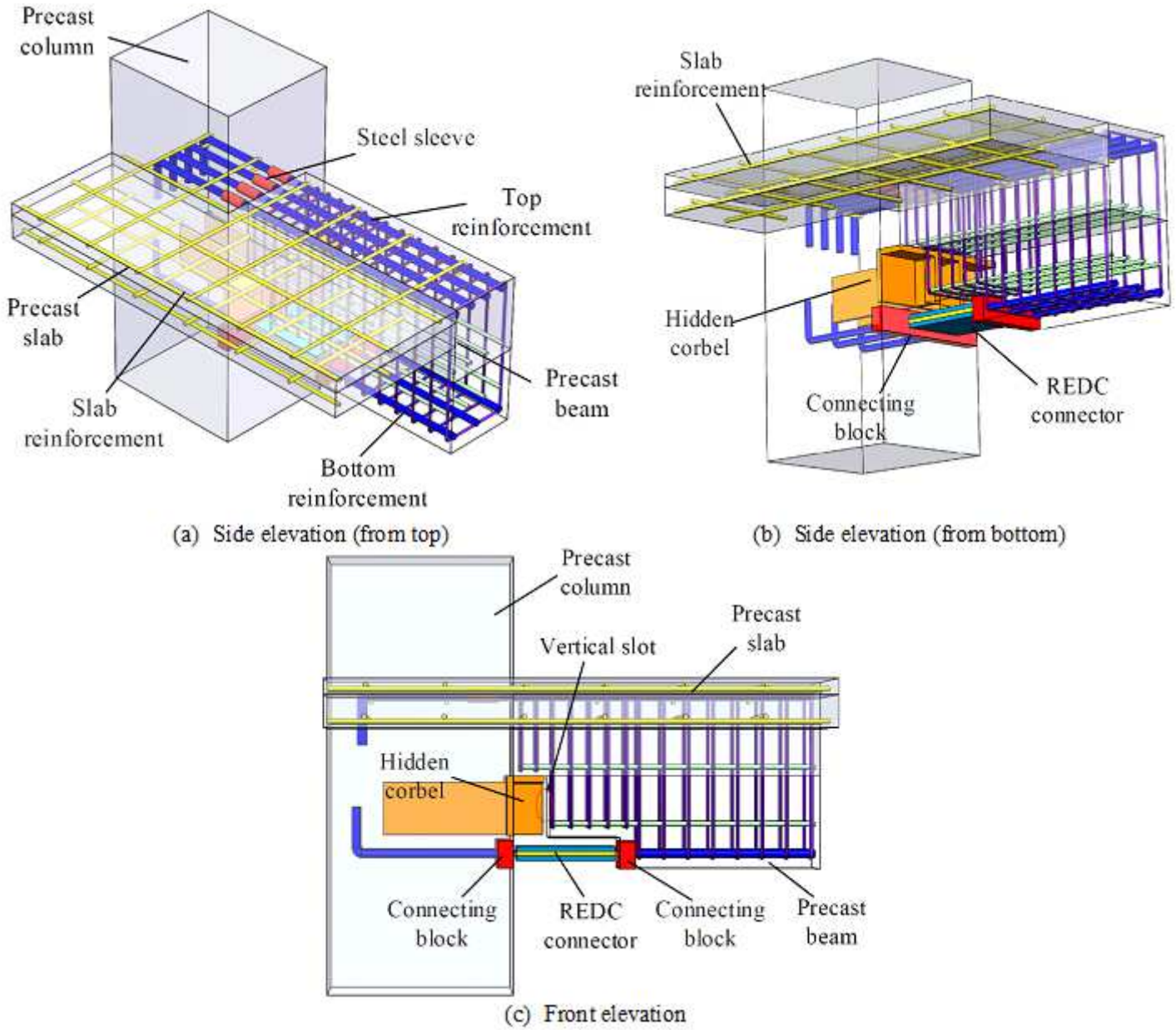


Figure 1

Description of the novel precast concrete beam-column connections with the REDC

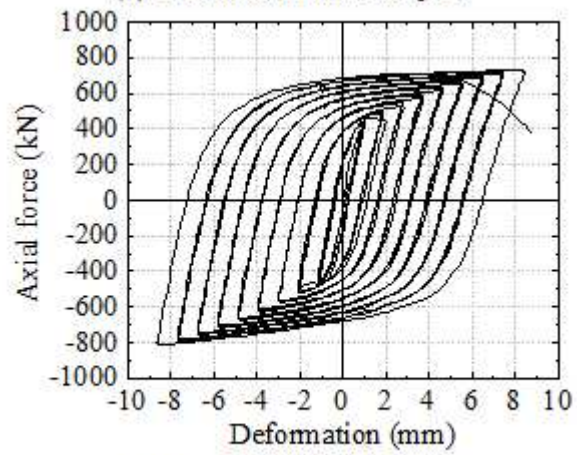
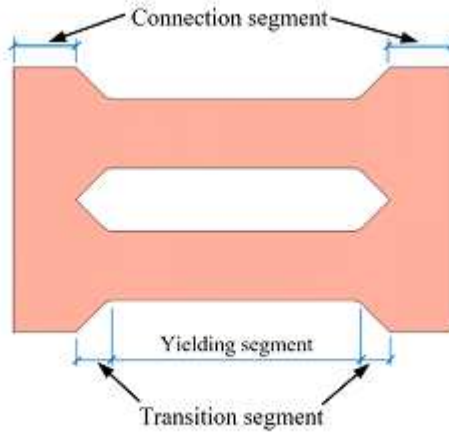
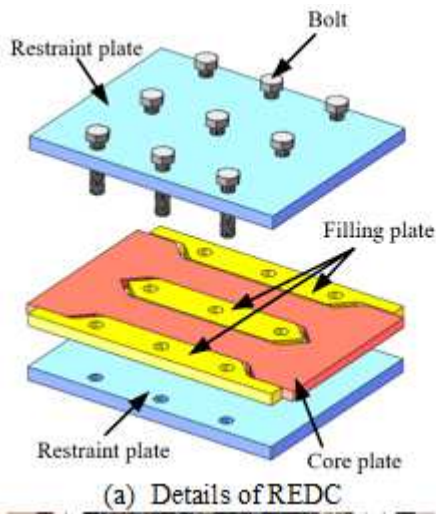


Figure 2

Details and test of REDC

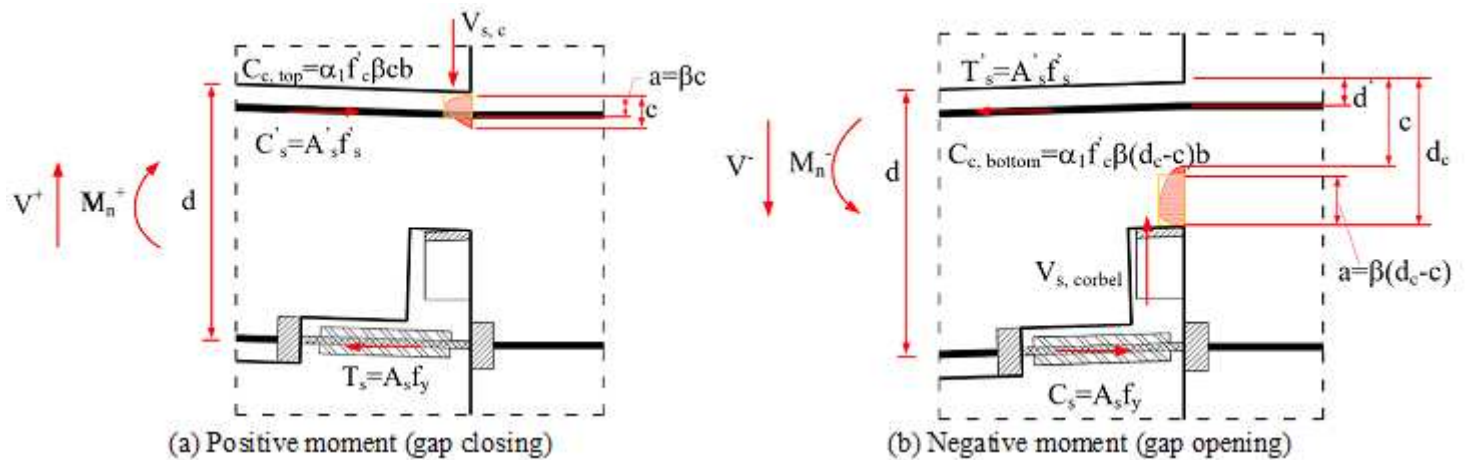


Figure 3

Force distribution in the connection under positive and negative bending

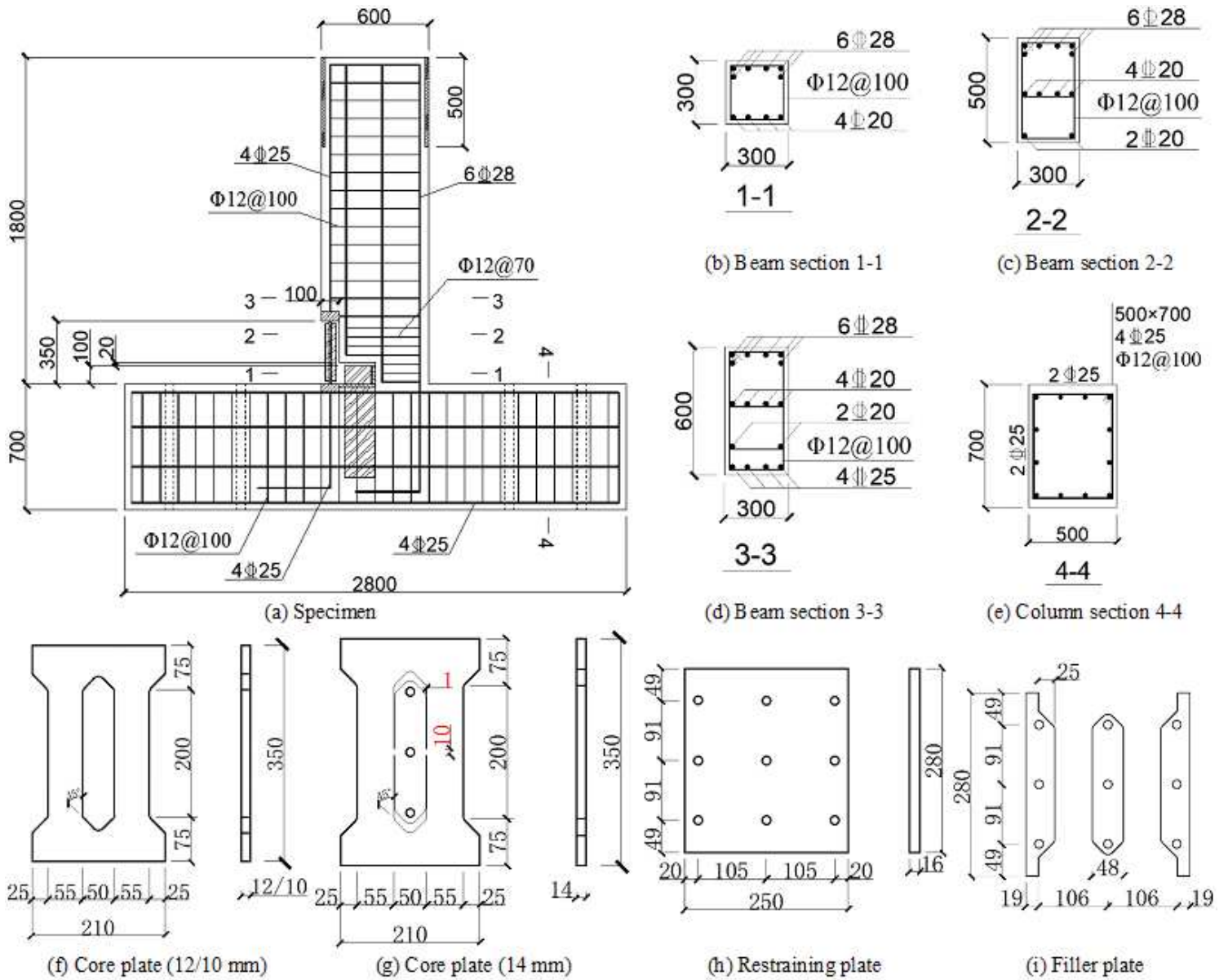


Figure 4

Details of the tested connections (all dimensions have units of mm)

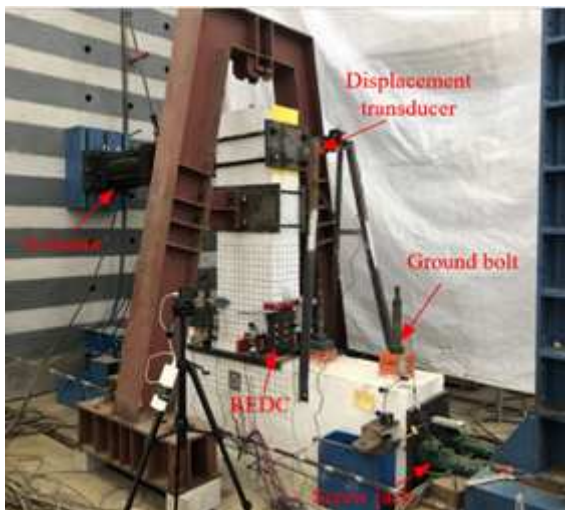


Figure 5

The specimen under test

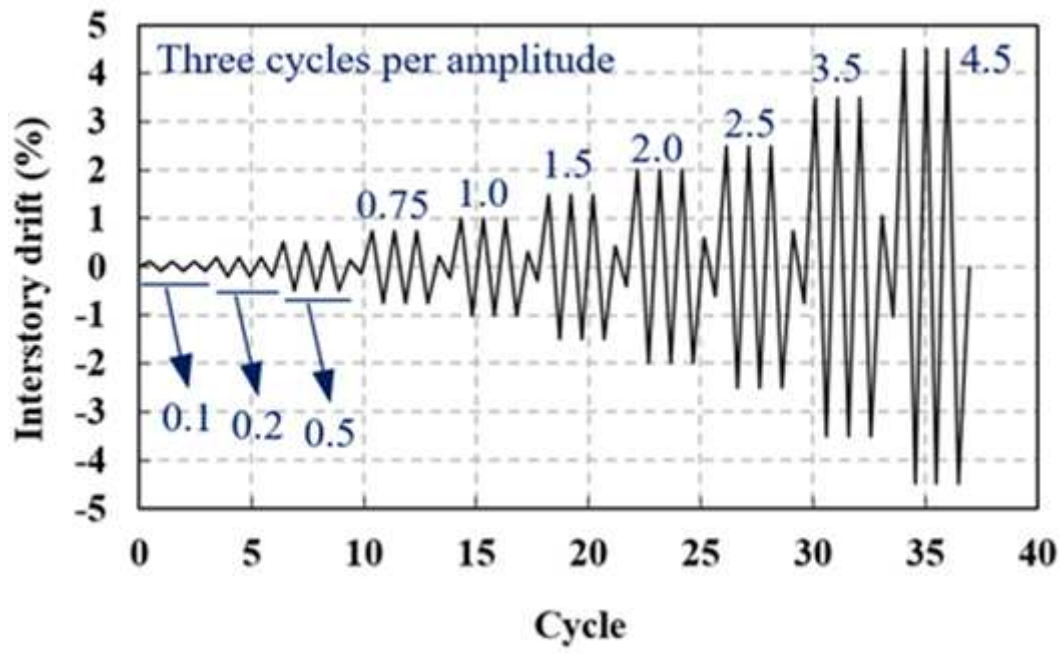


Figure 6

Quasi-static loading

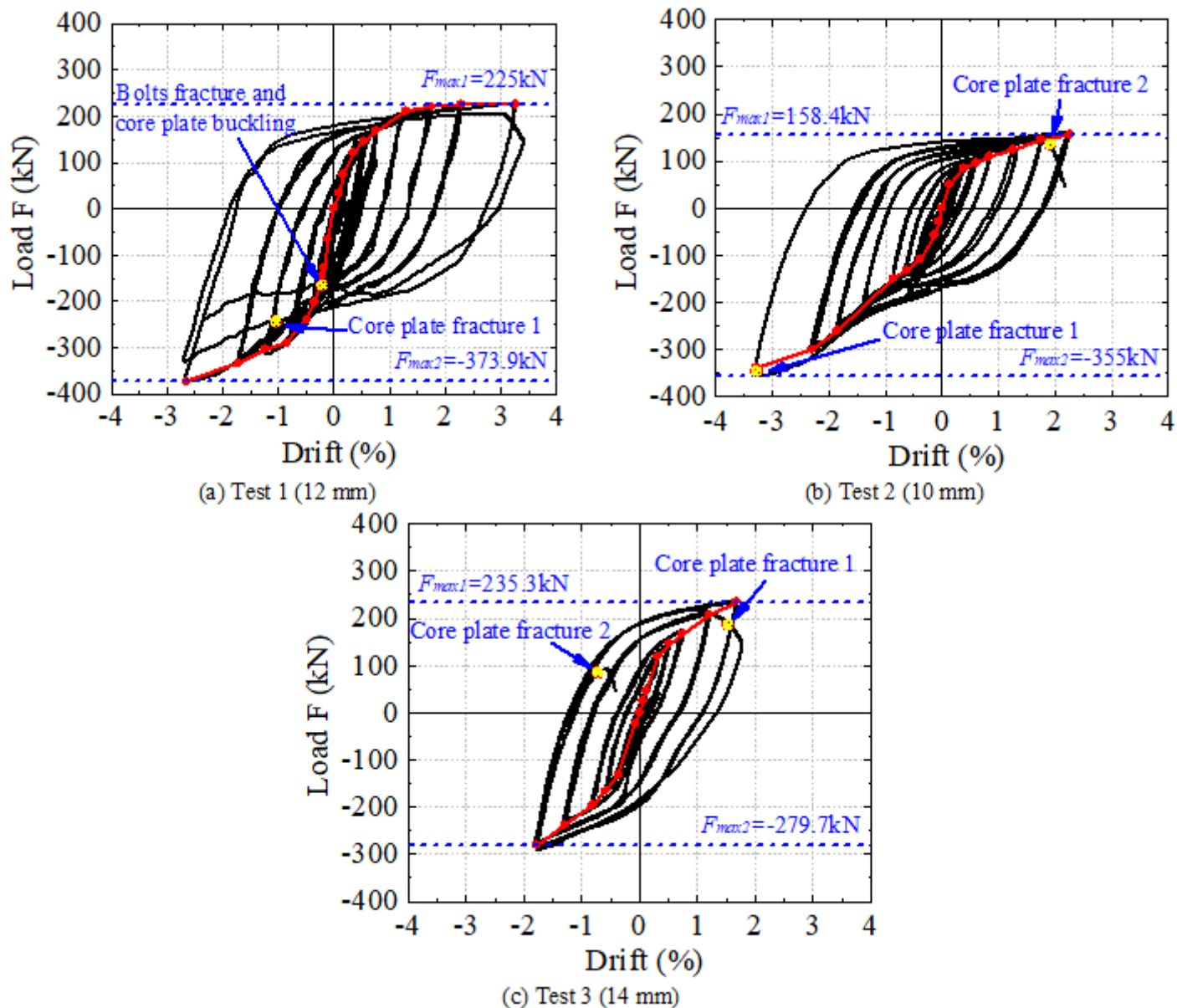
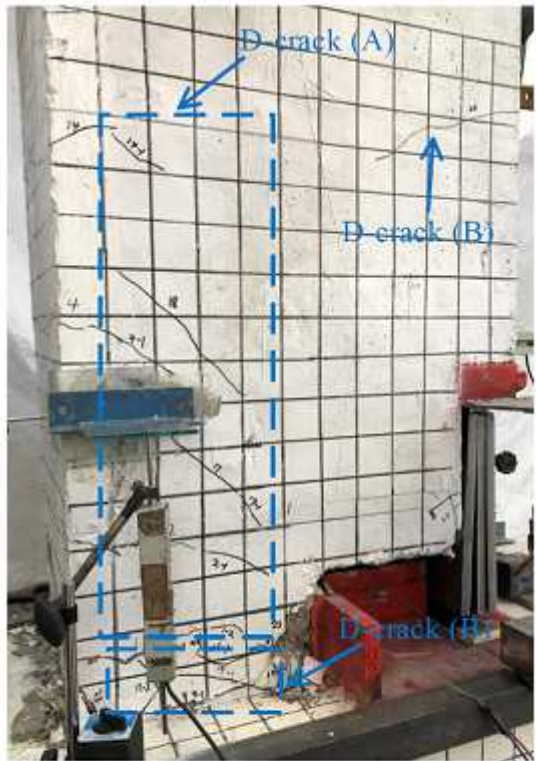


Figure 7

Load versus drift response for the SYPC connection: (a) Test 1; (b) Test 2; (c) Test 3



(a) Test 1 (front elevation)



(b) Test 1 (back elevation)



(c) Test 3 (front elevation)



(d) Test 3 (back elevation)

Figure 8

Cracking patterns at the ultimate condition

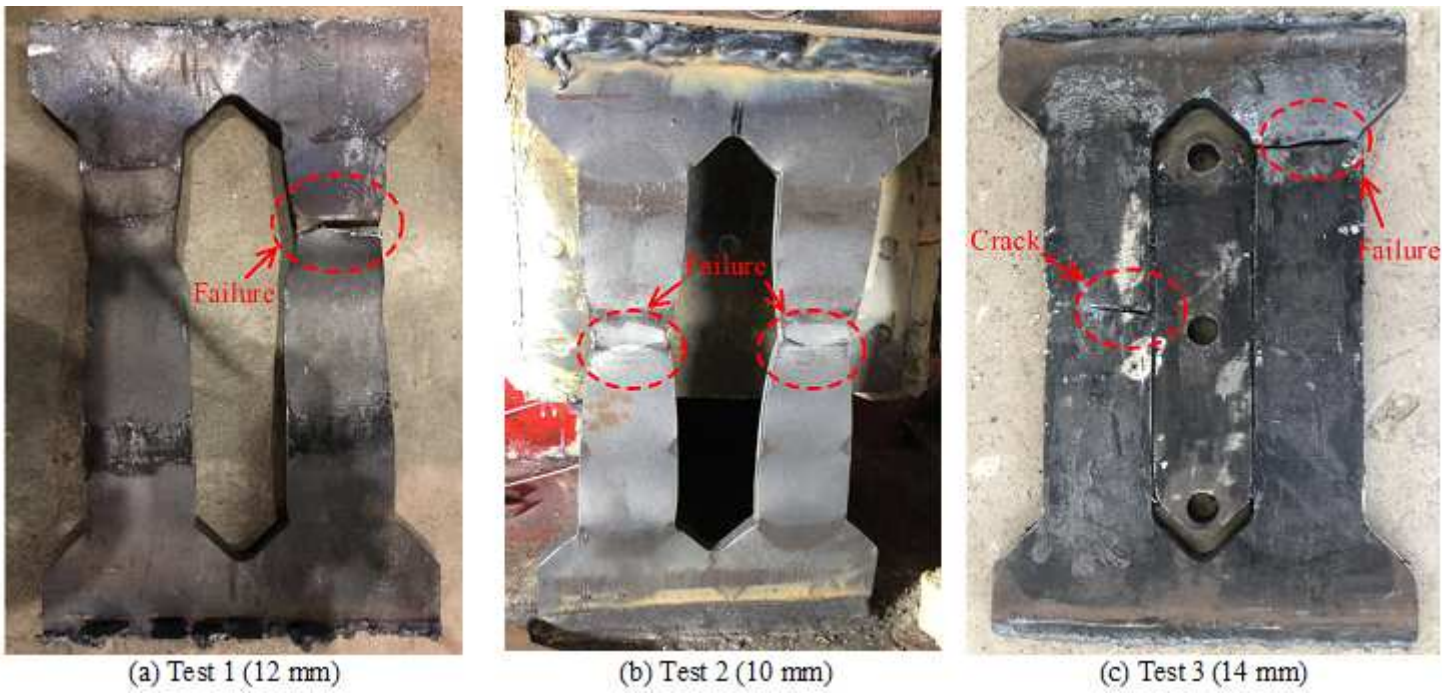


Figure 9

Failure pattern of the core plate



Figure 10

Buckling restraint state of the REDC

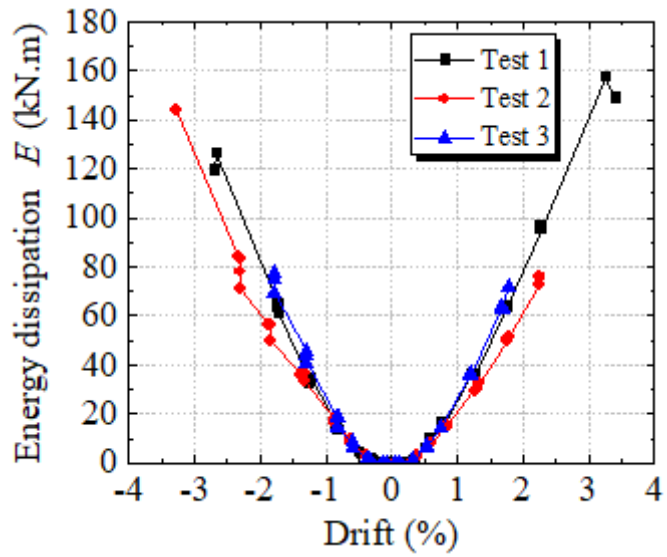


Figure 11

Energy dissipation per cycle versus drift ratio.

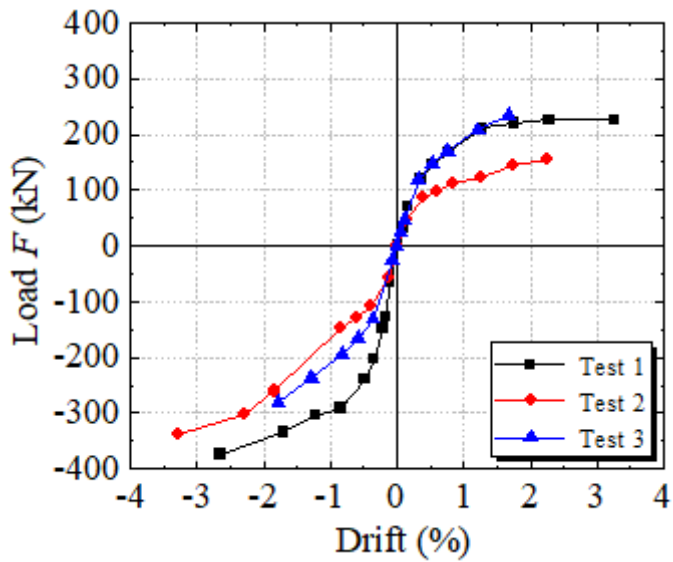


Figure 12

Skeleton curve

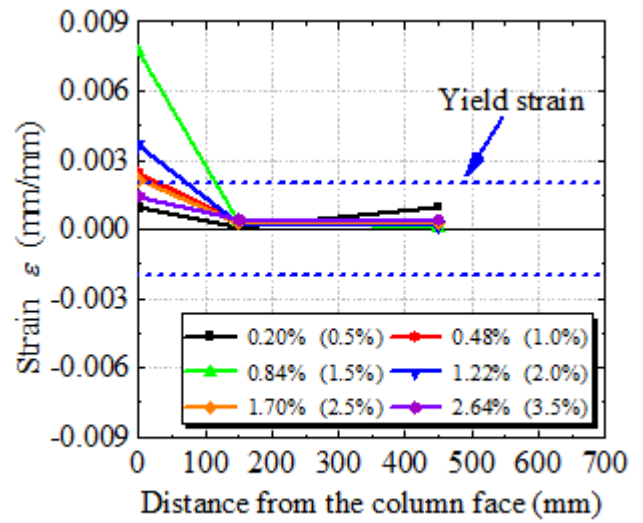
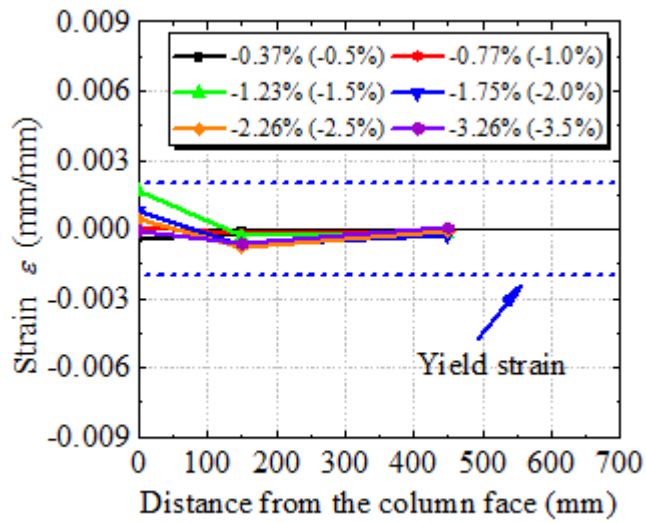


Figure 13

Strain profiles of the top reinforcement in Test 1

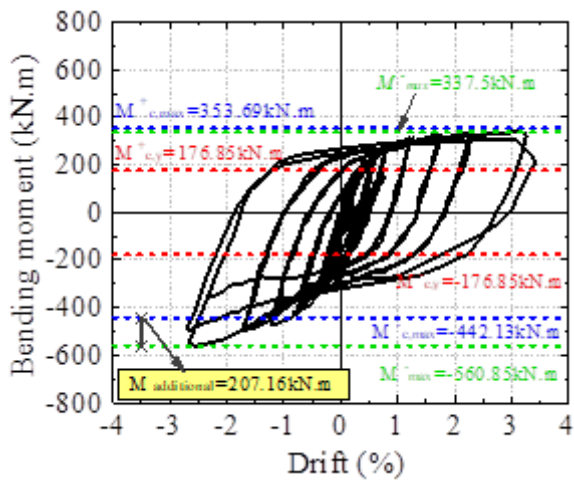


Figure 14

Schematic diagram of additional bending moment.

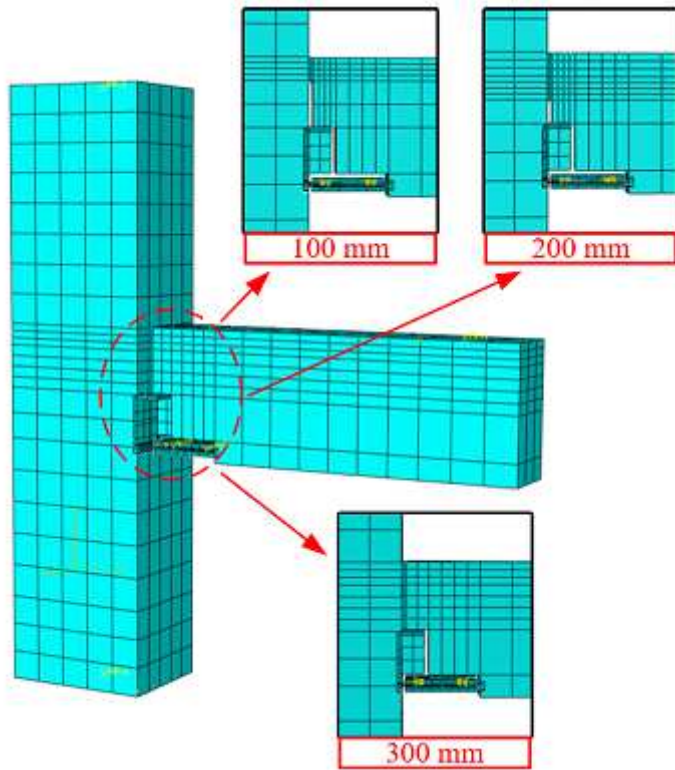


Figure 15

ABAQUS model for the novel precast connection

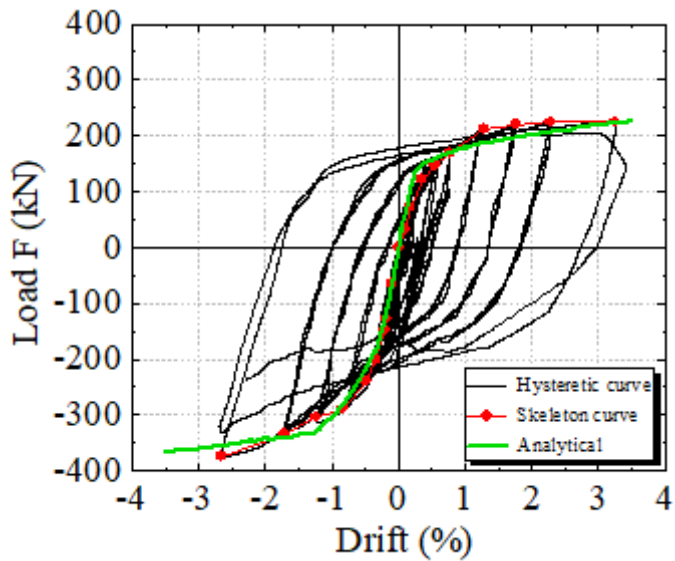


Figure 16

Comparison of analytical and experimental results

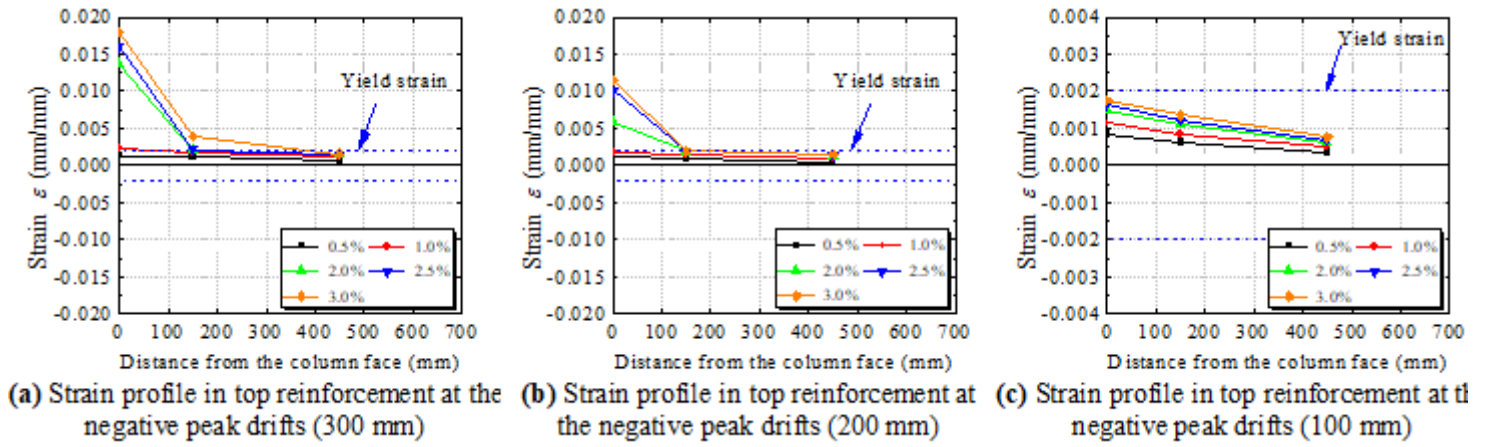


Figure 17

The peak strain of the top longitudinal reinforcement corresponding to each positive peak drift in the three models

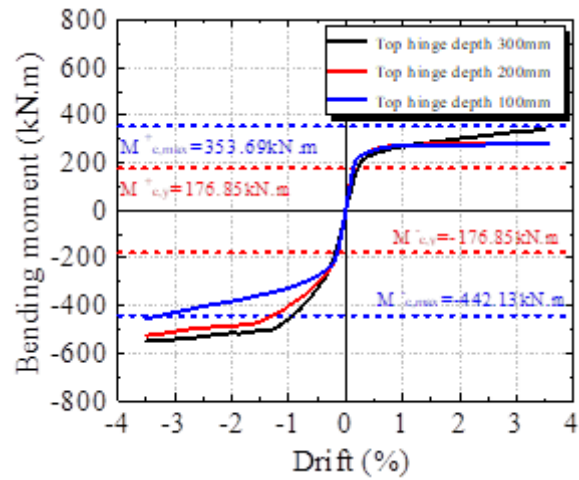


Figure 18

The comparison of the bending moment

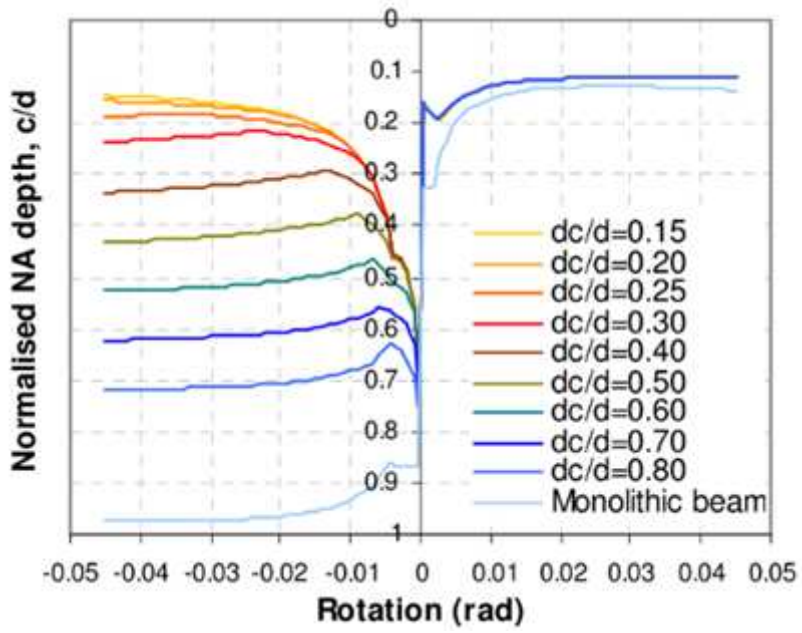


Figure 19

Parametric study for the concrete top-hinge depth (Au 2010)